# Clues from ab initio calculations on titanium isotopic fractionation in tholeiitic and calc-alkaline magma series

Sarah M Aarons, Nicolas Dauphas, Marc Blanchard, Hao Zeng, Nicole Xike X Nie, Aleisha C Johnson, Nicolas D Greber, Timo Hopp

# Clues from *ab initio* calculations on titanium isotopic fractionation in tholeiitic and calc-alkaline magma series

**Sarah M. Aarons[1,2*], Nicolas Dauphas[1], Marc Blanchard[3], Hao Zeng[1], Nicole Xike Nie[4], Aleisha C. Johnson[1], Nicolas D. Greber[5], Timo Hopp[1]**

[1]Origins Laboratory, Department of the Geophysical Sciences and Enrico Fermi Institute, The University of Chicago, Chicago, IL, 60637, USA
[2]Scripps Institution of Oceanography, University of California San Diego, CA, 92093, USA
[3]Géosciences Environnement Toulouse (GET), Observatoire Midi-Pyrénées, Université de Toulouse, CNRS, IRD, CNES, UPS, 14 avenue Edouard Belin, 31400 Toulouse, France
[4]Earth and Planets Division, Carnegie Institution of Science, Washington DC, 20015, USA
[5]Institute of Geological Sciences, University of Bern, 3012, Bern, Switzerland

*Corresponding author: Sarah Aarons (smaarons@ucsd.edu)

Keywords: *titanium, isotopes, fractional crystallization, isotopic fractionation, ab initio*

## Abstract

Magmatic differentiation produces positive correlations between $\delta^{49}$Ti and $SiO_2$. The equilibrium Ti isotope fractionation factors of Ti-bearing minerals are essential for understanding the mechanisms driving this isotopic fractionation. We present *ab initio* derived mean force constants of Ti-bearing minerals (barium orthotitanate, potassium titanium oxide, fresnoite, diopside, geikielite, karooite, titanite, pseudobrookite, anatase, and titanium oxide) based on density functional theory (DFT) to calculate equilibrium isotopic fractionation factors. We find that the main driver for Ti isotopic fractionation is its coordination, with 4-, 5-, and 6-fold coordinated Ti characterized by mean force constants of 547, 462, and 310 N/m respectively. The coordination number of Ti in silicate melts is thought to be lower than in minerals, driving magmas towards higher $\delta^{49}$Ti values by fractional crystallization. The mineral-melt fractionation factors allow modeling of the observed Ti isotope trends in tholeiitic and calc-alkaline rocks. Our model results indicate that to first order, the steeper $\delta^{49}$Ti trend observed in tholeiitic *vs.* calc-alkaline magmas is most likely due to enhanced removal of Ti into sequestered minerals at low $SiO_2$ concentration in tholeiitic series compared to calc-alkaline series. The $\delta^{49}$Ti-$SiO_2$ differentiation trends however depend on Ti coordination in the melt and the strengths of Ti bonds in diverse Fe,Ti-oxides, which are still uncertain. Our results show that Ti isotopes can be used to reconstruct the crystallization history and identify the magmatic series parentage of magmas that otherwise lack context, but further work is needed to identify the drivers behind Ti isotopic fractionation in igneous rocks.

## 1. Introduction

Arc magmatism and calc-alkaline magma differentiation are fundamental processes in the establishment of felsic continental crust [1, 2 3-5]. Titanium (Ti) isotopes provide unique insights into magmatic differentiation processes, as the $\delta^{49}$Ti composition of magmatic rocks increases with increasing silica content, reflecting the history of partial melting and Fe-Ti oxide crystallization[6-12]. The Ti isotopic composition of fine-grained terrigenous sediments (shales) has been used to conclude that, as far back as 3.5 Ga, the composition of the crust exposed to weathering comprised a large fraction of felsic rocks, implying

that subduction processes were likely operating before that time[9]. Subsequent work demonstrated that Ti isotopes fractionated distinctly in plume and island arc settings[7, 11, 12], suggesting that Ti isotopes may provide insights into the geodynamic setting responsible for the formation of continental crust [13].

In general, igneous rocks display a monotonically increasing trend in $\delta^{49}$Ti during magmatic differentiation, which is attributed to the fractionation of Ti isotopes following the saturation and crystallization of Ti-bearing oxides [6, 7, 10-12]. However, different rock series show contrasting behaviors in Ti isotope fractionation during tholeiitic and calc-alkaline magmatic differentiation, and the process responsible for these trends is still not well understood. Modern calc-alkaline magmas occur in subduction zone environments and are characterized by enrichment in water content, higher oxygen fugacity, and Fe depletion [14-19]. Tholeiitic magmas can occur in both subduction and intraplate environments and are characterized by strong Fe and Ti enrichments and lower water content and oxygen fugacity [14, 15].

Several studies have focused on stable Fe isotopes in a variety of magmatic systems [e.g., [20-24]], and only one thus far which has reported both stable Ti and Fe isotopic compositions [13]. The isotopic variations documented thus far reflect the combined effects of mineral-melt equilibrium involving silicates and oxides (modulated by Fe redox state and coordination), and kinetic effects associated with Fe-Mg interdiffusion in olivine. Due to these multiple controls, interpretation of Fe isotopic variations of bulk differentiated igneous rocks is often far from straightforward, unless individual mineral analyses are performed and a full differentiation series is studied.

The increase in $\delta^{49}$Ti values with increasing $SiO_2$ in all magmatic series[6, 7, 10-12] was hypothesized[6] to be the result of the preferential incorporation of light Ti isotopes into 6-fold coordinated Fe-Ti oxides during fractional crystallization, whereas the silicate melt hosts Ti in lower coordination averaging ~4.5 to 5.4[25, 26]. Lower coordinated bonding environments are indeed associated with stronger and stiffer bonds, which promote heavy isotope enrichments at equilibrium[27]. During crystallization, heavy Ti isotopes

preferentially remain in the low-coordination melt, while light Ti isotopes are incorporated into crystallizing 6-fold coordinated Ti-bearing mineral phases [6].The hypothesis that Fe-Ti oxide crystallization drives Ti isotopic fractionation during magmatic differentiation was confirmed by Johnson *et al.*[11], who separated Fe-Ti oxides from Kīlauea Iki Lava Lake (primarily ilmenite and Ti-magnetite) using heavy liquid separation, and then measured the Ti isotopic composition of the oxide and glass. They found that Fe-Ti oxide separates were isotopically lighter than their glass counterparts[11]. Several studies have since shown that a single melt-crystal equilibrium fractionation factor cannot account for the isotopic variations that have been documented in magmatic series, even when the temperature decrease in more evolved magmas is accounted for[7, 11, 12]. Three possible explanations for the non-constant oxide-melt isotopic fractionation factor are: (*i*) the fractionation is not solely of equilibrium origin but also involves kinetic effects such as diffusion [28, 29], (*ii*) the fractionation is influenced by the coordination number of Ti in the melt, which tends to decrease with increasing differentiation [25], and (*iii*) the fractionation is influenced by the composition of the oxides that crystallize [12]. To test these three possibilities, it is important to predict how Ti isotopes can be fractionated between co-existing phases at equilibrium. In the present contribution, we use an *ab initio* DFT approach to calculate a new set of Ti equilibrium fractionation factors aimed at understanding the drivers behind Ti isotopic fractionation in igneous rocks. Wang *et al.*[30] and Leitzke *et al.*[31] previously calculated the equilibrium Ti isotopic fractionation factors of $Ti^{4+}$-bearing clinopyroxene, orthopyroxene, olivine, pyrope, rutile, karrooite, as well as $Ti^{3+}$-bearing clinopyroxene. We extend this work here to include $Ti^{4+}$-bearing $BaTiO_4$, $K_2Ti_2O_5$, Ti-diopside, geikielite, karrooite, titanite, pseudobrookite, fresnoite, anatase, and $Ti^{3+}$-bearing Ti oxide. Some of the minerals (fresnoite, barium orthotitanite, and the average of 6-fold coordinated minerals) are used as proxies for Ti coordination in silicate melt. These fractionation factors are then used to evaluate how Ti isotopes can be fractionated differently in the two main magma series: calc-alkaline and tholeiitic.

### 1.2 Petrologic controls on Ti during magmatic differentiation

Tholeiitic series are found in plume, mid-ocean ridges, and arc settings, while calc-alkaline series are encountered almost exclusively in convergent arc-settings[15, 32]. Calc-

alkaline magmas are noted for their higher water contents, higher oxygen fugacities ($fO_2$), and lower Ti contents; which are by-products of subduction [18, 19, 33]. Calc-alkaline magmas typically also have higher initial $SiO_2$ contents due to their production through water-induced flux melting of the mantle [34]. The criteria for distinguishing between these series are mainly based on the behavior of Fe during differentiation. The divergence in Fe behavior is due to the sequence and rate of mineral crystallization [5], which also influences the behavior of Ti. However, unlike Fe whose behavior is influenced by the oxygen fugacity and crystallization of both mafic silicate and oxide minerals, Ti is predominantly affected by Fe-Ti oxides such as Ti-magnetite and ilmenite.

In tholeiitic series, the crystallization sequence is olivine, plagioclase feldspar and clinopyroxene (augite), with plagioclase crystallization dominating the mineral assemblage of crystallizing phases. Early on in the differentiation of tholeiitic series, the removal of high MgO/low FeO mafic minerals like olivine and pyroxene increases the total FeO content. At the same time, the removal of these $SiO_2$-poor mafic minerals is partially compensated by the removal of $SiO_2$-rich plagioclase, so that the $SiO_2$ content of the melt remains more or less constant [14, 35]. The FeO content reaches a peak, and $SiO_2$ remains approximately constant, prior to saturation and crystallization of spinels and Fe-Ti oxides. The FeO content then rapidly decreases while the $SiO_2$ content increases because the crystallizing phases are relatively FeO-rich and $SiO_2$-poor. At this point, the crystallization of plagioclase decreases and is less important in driving the chemical evolution of the magma. In contrast, the presence of water and higher $fO_2$ in the calc-alkaline series suppresses plagioclase crystallization and results in an early onset of spinel and oxide crystallization, which drives the $SiO_2$ content to increase rapidly during the early stages of differentiation while the total FeO content does not increase as dramatically as is observed in the tholeiitic series[14, 15, 17].

The difference in Fe behavior during differentiation controls the timing of spinel and Fe-Ti oxide saturation and crystallization, as well as the pace at which Ti is removed relative to the evolution of the melt with respect to $SiO_2$. This behavior has important implications for the Ti isotopic composition and evolution of tholeiitic and calc-alkaline

magmas, as the trajectory and evolution of Ti isotope compositions during differentiation should be primarily driven by Ti isotopic fractionation between melt and Ti-bearing minerals, notably Fe-Ti oxides. Titanium isotopes therefore have the potential to inform us on the history of oxide crystallization and may be related to water content, $fO_2$, pressure, and initial geochemical composition of magmas during magmatic differentiation.

## 2. Method

### 2.1 Equilibrium isotopic fractionation factors

To address the question of how and why Ti isotopes fractionate differently during differentiation of tholeiitic and calc-alkaline magmas, we calculated through an *ab initio* density functional theory (DFT) approach the mean force constant ($\langle F \rangle$ in N/m) of Ti bonds in various minerals from which equilibrium isotopic fractionation factors can be calculated as a function of temperature. We specifically focused on minerals relevant to magmatic systems and some exotic crystals in which Ti is present in a range of coordination environments. Wang *et al.* [30] and Leitzke *et al.* [31] also reported isotopic fractionation factors in a variety of Ti bearing phases using DFT, and their results are compared with ours below.

The Ti isotopic composition is hereafter reported in $\delta^{49}$Ti notation, which is the permil deviation from the $^{49}Ti/^{47}Ti$ ratio of the Origins Laboratory Ti reference material (OL-Ti), which has a near-chondritic composition [10],

$$\delta^{49}\mathrm{Ti}\ (‰) = \left[\frac{\left(^{49}\mathrm{Ti}/^{47}\mathrm{Ti}\right)_{\mathrm{Sample}}}{\left(^{49}\mathrm{Ti}/^{47}\mathrm{Ti}\right)_{\mathrm{OL\text{-}Ti}}} - 1\right] \times 1000. \quad \text{(eq. 1)}$$

Minerals modeled in this work include $Ti^{4+}$-bearing barium orthotitanate (IV coordination), potassium titanate (V), fresnoite (V), anatase (VI), diopside (VI), geikielite (VI), karrooite (VI), titanite (VI), pseudobrookite (VI), and $Ti^{3+}$-bearing titanium oxide (VI). Additionally, Ti-magnetite (VI), ulvöspinel (VI), and ilmenite (VI) were also calculated but the structures were dynamically unstable, and the results cannot be trusted,

so we do not report those results in the present contribution. We nevertheless describe briefly the unsuccessful attempts that we have made at solving this issue of dynamical instability to avoid replication of these attempts by future studies. Mineral structures were sourced from experimental data (described below in subsection *Mineral Structures*), reduced to primitive cells if possible, and their lattice parameters and atomic positions were relaxed until the residual forces on atoms and pressure were smaller than $10^{-4}$ Ry/au and 0.1 kbar.

A phonon calculation was then performed for each structure and partial phonon density of states (PDOS) for Ti (and all other elements) were calculated and averaged if more than one Ti atom was present in the unit cell (see Supplementary file S1). The average force constants for the Ti-bearing mineral phases were calculated using the formula [36]:

$$\langle F \rangle = \frac{M}{\hbar^2} \int_0^\infty g(E)\, E^2 dE, \qquad \text{(eq. 2)}$$

where $\langle F \rangle$ is the force constant of the Ti bonds in the mineral of interest in N/m, $M$ is isotope mass, ħ is the reduced Planck constant, $g(E)$ is the PDOS, and $E$ is the vibration energy. The reduced partition function ratio (*rpfr* or $\beta$-factor) of a mineral, which corresponds to the equilibrium fractionation between the mineral phase and monoatomic gaseous Ti, can be written as a polynomial of the even powers of the inverse of the temperature, with the coefficients given by the even moments of $g(E)$[36],

$$1000 \ln \beta = \frac{A_1}{T^2} + \frac{A_2}{T^4} + \frac{A_3}{T^6}. \text{ (eq. 3)}$$

At high temperature the first term ($A_1$) dominates the *rpfr* for $^{49}$Ti/$^{47}$Ti. Using the methods described in [36, 37] we can calculate the $\beta$-factors for Ti using the masses of the isotopes (*i.e.*, $^{49}$Ti and $^{47}$Ti), the Boltzmann constant, and the Planck constant. For the ratio $^{49}$Ti/$^{47}$Ti, this equation becomes,

$$1000 \ln \beta_{^{49}\mathrm{Ti}/^{47}\mathrm{Ti}} \simeq 3815 \frac{\langle F \rangle}{T^2}. \text{ (eq. 4)}$$

Below, we apply the fractionation factors calculated by *ab initio* to MELTS models of magmatic differentiation of tholeiitic and calc-alkaline magmas to understand the driving factors responsible for the contrasting behavior of Ti isotopes between the two series. We are well aware that magma mixing and assimilation play significant roles in the petrogenesis of differentiated igneous rocks, notably calc-alkaline series[5, 38] but fractional crystallization remains the main driver [39, 40] and we will therefore focus on this end-member scenario.

**2.2 Mineral Structures for DFT Calculation**

We studied titanate, oxide, and silicate minerals where $Ti^{3+}$ or $Ti^{4+}$ is four-, five-, and six-fold coordinated with oxygen atoms (Fig. 1). Several uncommon minerals were investigated as they host Ti in special coordination environments that resemble those encountered in silicate melts [25].

*$Ti^{4+}$ in 4-fold coordination:* In barium orthotitanate ($Ba_2TiO_4$), $Ti^{4+}$ is tetrahedrally (4-fold) coordinated. The monoclinic cell used contains four times the structural formula (Z=4, space group $P2_1/n$) [41].

*$Ti^{4+}$ in 5-fold coordination:* In potassium titanate ($K_2Ti_2O_5$), $Ti^{4+}$ is five-fold coordinated in a monoclinic cell with the coordination environment being a trigonal bipyramid (Z=1, space group C12/m1) [42]. Titanium *K*-edge X-ray adsorption near edge structure spectroscopy (XANES) and extended X-ray absorption fine structure (EXAFS) measurements showed that 5-fold coordinated Ti in silicate melt most closely resembles fresnoite, $Ba_2TiO(Si_2O_7)$, a mineral in which Ti is coordinated in a square base pyramid with a Ti-O bond at the apex (Z=2, space group P4bm)[43].

*$Ti^{4+}$ in 6-fold coordination:* The majority of minerals, including geikielite, karrooite, pseudobrookite, titanite, anatase, and diopside have Ti in six-fold coordination. The motivation for modeling geikielite ($MgTiO_3$) is the fact that DFT calculations of ilmenite ($FeTiO_3$) yielded dynamically unstable structures as indicated by the presence of imaginary frequencies. For geikielite ($MgTiO_3$, space group R-3 [44]), we used the

primitive rhombohedral cell (Z=2). Karrooite ($MgTi_2O_5$)[45] and pseudobrookite ($Fe^{3+}{}_2Ti^{4+}O_5$) are both orthorhombic, space group Cmcm [46]. Pseudobrookite displays an antiferromagnetic ordering. Titanite has a monoclinic cell where $Ti^{4+}$ occupies the octahedral sites ($CaTiSiO_5$, Z=4, space group $P2_1/c$) [47]. Anatase ($TiO_2$, tetragonal space group $I4_1/amd$, Z=4) also displays 6-fold coordinated $Ti^{4+}$, and Ti-diopside has a monoclinic cell where $Ti^{4+}$ occupies the octahedral sites ($Ti^{4+}Si_2O_6$, space group -C 2yc)[48].

*$Ti^{3+}$ in 6-fold coordination:* The last compound considered is titanium oxide ($Ti_2O_3$) where $Ti^{3+}$ displays a six-fold coordination. We chose this last compound to investigate the role of high coordination number and low oxidation state on the force constant. This compound was modeled using the primitive rhombohedral cell (space group R-3c, Z = 2) [49].

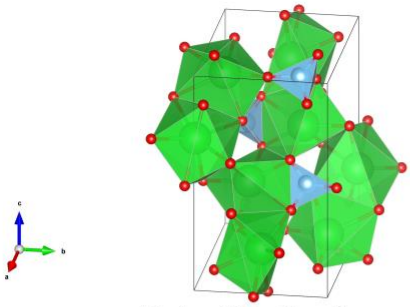

Barium Orthotitanate

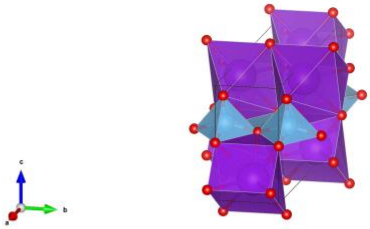

Potassium titanite

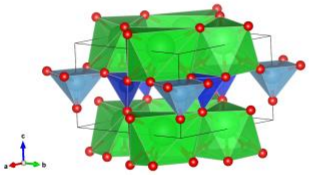

Fresnoite

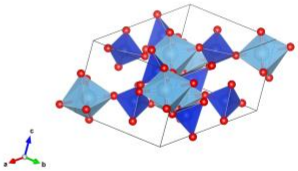

Ti-Diopside

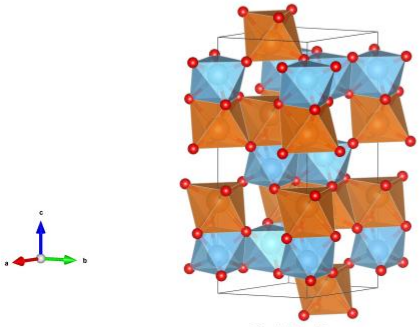

Geikielite

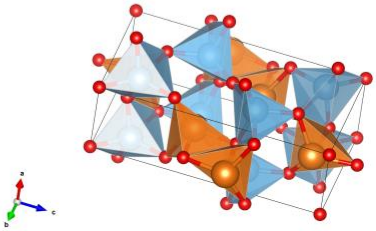

Karrooite

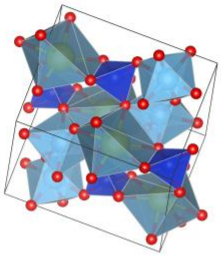

Titanite

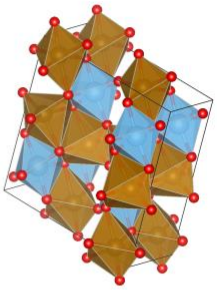

Pseudobrookite

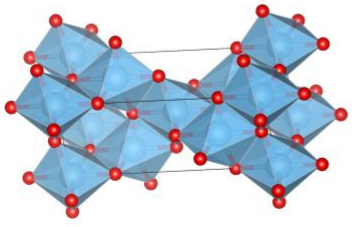

Anatase

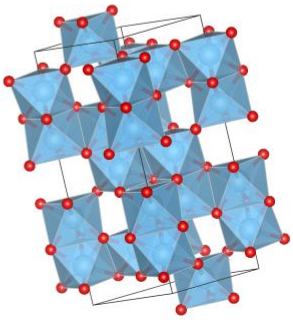

Titanium oxide

**Fig. 1.** Structures (rendered by VESTA)[50] of Ti-bearing minerals investigated here. Red circles represent O, orange represents Mg, light blue represents Ti, dark blue represents Si, gold represents Fe, green represents Ba, purple represents K, and yellow represents Ca.

### 2.3. *Ab initio* calculations

All *ab initio* computations were performed with Quantum ESPRESSO [51] with plane-wave basis sets, Perdew, Burke and Ernzerhof (PBE) generalized gradient approximation (GGA) functionals [52], and norm-conserving pseudopotentials from ONCV library [53]. The kinetic energy and charge-density cutoff were set at 85 and 340 Ry respectively for all systems. Monkhorst k-point and q-point grids [54] were chosen to be 4×4×2, 2×2×2 for barium orthotitanate, 4×4×4, 3×3×3 for potassium titanate, 4×4×4, 2×2×2 for diopside, 3×3×3, 3×3×3 for geikielite, 4×4×2, 2×2×2 for karrooite, 3×3×3, 2×2×2 for titanite, 4×4×2, 2×2×2 for pseudobrookite, 4×4×4, 3×3×3 for titanium oxide, 2×2×2, 2×2×3 for fresnoite, 8×8×8, 2×2×2 for anatase. Calculated (cal.) and experimental (exp.) crystal lattice parameters of each mineral are shown in Table 1.

### 2.4 Melt coordination

The main driver behind the fractionation of Ti isotopes during magmatic differentiation is expected to be the difference in coordination between the Ti-bearing minerals and the silicate melt [6]. The coordination environment of Ti in silicate melts is, however, not well constrained. Titanium XANES and EXAFS have been used to characterize the coordination of Ti in synthetic and natural materials but for the most part, the glass and melt compositions studied are quite far from those that we are interested in for application to Ti high-temperature isotopic geochemistry.

Farges and Brown [25] measured a series of glass samples that were either natural, or synthetic but with natural compositions. These samples were measured both below the glass transition and above the liquidus. In all glasses, $^{[5]}$Ti dominated but the more mafic samples contained 30-50% of $^{[6]}$Ti while the more felsic samples contained 30-60% of

[4]Ti. Among the igneous rocks measured by Farges and Brown [25], the average coordination ranged from 5.4 in basalt to 4.5 in rhyolite. No drastic or systematic change in Ti coordination was seen when the glasses were melted. The volatile content (F, Cl, $H_2O$) also seemed to have a limited effect on Ti coordination in glasses/melts. The primary control on Ti coordination seemed to be the degree of polymerization of the silicate glass/melt, with a higher proportion of non-bridging oxygen per silicon tetrahedron associated with a lower coordination. The nature of the network modifiers (Na, K, Ca) also seemed to affect the coordination of Ti, with larger cations favoring a lower coordination. In Figure 2, we plot the calculated non-bridging oxygen to tetrahedron (NBO/T) of the Rhyolite MELTS simulations (this study) and the relationship between NBO/T and Ti coordination from Farges and Brown [25]. At a given $SiO_2$ content, tholeiitic magmas have higher NBO/T ratio compared to calc-alkaline magmas with a generally decreasing trend during magmatic differentiation (Fig. 2a). It is therefore conceivable that difference in Ti coordination between tholeiitic and calc-alkaline magmas could influence how Ti isotopes fractionate during magmatic differentiation. While the seminal study of Farges and Brown [25] identified the main parameters affecting Ti coordination in glasses and melts, the data are too scant to predict the exact coordination of Ti in a silicate melt of a given composition.

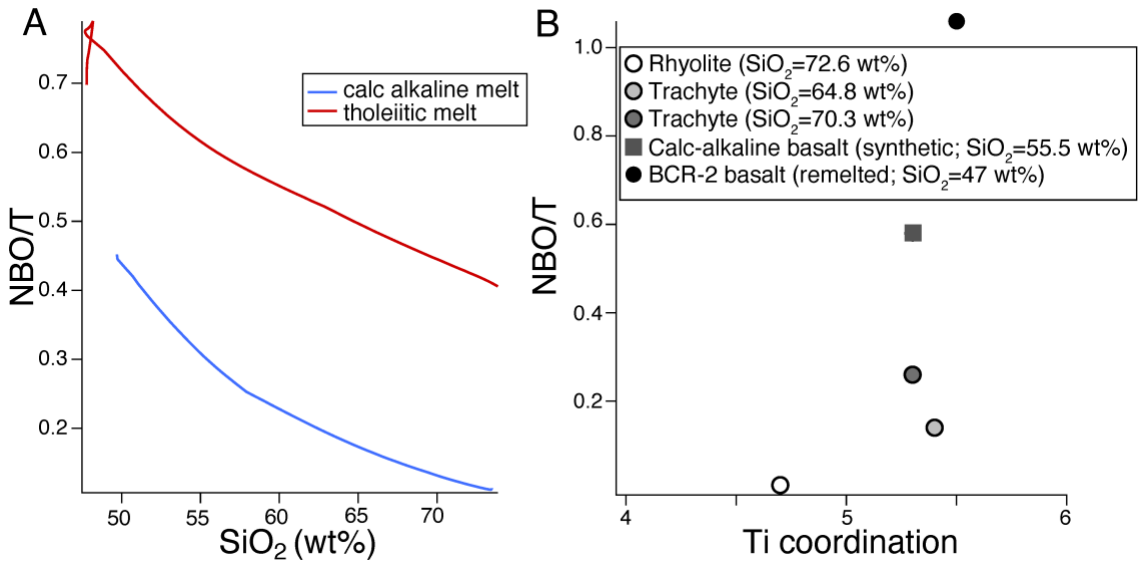


**Fig. 2 a)** Non-bridging oxygen per silicon tetrahedron (NBO/T) of tholeiitic (red line) and calc-alkaline (blue line) magmas with respect to silica content from Rhyolite MELTS simulations. **b)** NBO/T with respect to Ti coordination (basalt to rhyolite with an average

coordination ranging from 4.7 to 5.5) in glass samples measured by Farges and Brown [25]. Silica content of glasses are noted in the legend along with sample details.

Leitzke *et al.* [31] studied the coordination and oxidation state of Ti in various synthetic minerals and glasses to interpret measurements of Ti oxidation state and isotopic fractionation in lunar rocks. They used lunar basalt starting composition and the glasses quenched after partial melting and partial crystallization contained 42-51 wt% $SiO_2$ and Ti as 4+ and in 5-fold coordination. Their data on the coordination of Ti in lunar basaltic magmas are, however, of limited use for interpreting Ti isotopic variations in terrestrial rocks as they focused on mafic compositions very rich in titanium (~7-22 wt% $TiO_2$) and devoid of alkali elements (K and Na).

Overall, it seems like Ti is predominantly in 5-fold coordination with some contributions of 6-fold coordination in more mafic magmas and 4-fold coordination in more felsic magmas. According to Farges and Brown [25], Ti in 5-fold coordination in silicate glasses and melts seems to form titanyl bonds also encountered in natural minerals fresnoite, innelite, and lamprophyllite, where Ti is in a square base pyramid. We use the fresnoite structure to emulate Ti in 5-fold coordination in melts. We also calculated potassium titanate, as this mineral hosts Ti in a 5-fold trigonal bipyramid coordination [42], to provide a comparison with the 5-fold square pyramid coordination. Farges and Brown [25] did not detect any significant change in coordination below the glass transition and above the liquidus but further work is needed to assess to what extent the bond stiffness of Ti in proxy minerals approximates that of Ti in silicate melt, which may affect the Ti isotope fractionation modeled here. To address the possibility that the coordination of Ti in a silicate melt changes under different $SiO_2$ concentrations as noted in Farges and Brown[26], we model the evolution of a tholeiitic and calc-alkaline melt under three different scenarios:

(1) Ti in the melt is 100% 5-fold coordinated.
(2) Ti is 40% 6-fold and 60% 5-fold in mafic magmas (<52wt% $SiO_2$), 100% 5-fold in intermediate magmas (52-63 wt% $SiO_2$), and 45% 4-fold and 55% 5-fold in felsic (>63 wt% $SiO_2$) magmas.

(3) We assume that Ti coordination (and force constant) is primarily driven by melt polymerization and parameterize it as a linear function of NBO/T.

### 2.5 MELTS modeling

We used Rhyolite MELTS [55, 56] to simulate Ti isotopic fractionation during fractional crystallization. The starting compositions are primitive tholeiitic and calc-alkaline compositions from [6, 11]. We tracked the compositions of the melt and minerals during fractional crystallization. For tholeiitic series simulations, crystallization starts at a liquidus temperature of 1215 °C and the simulation is run down to 845 °C in decrements of 5 °C, with the pressure set at 0.6 kbar [11]. For calc-alkaline series simulations, the temperature decreases from 1120 °C to 760 °C and the pressure is set at 1 kbar [6]. The initial oxygen fugacities of the tholeiitic and calc-alkaline melts were set at QFM -0.3 and +0.6, respectively. In both cases, the melts evolved with no oxygen fugacity buffer and at constant pressure. We explored the effect of buffering the oxygen fugacity but did not find a drastically different evolution for modeled Ti isotope composition for realistic buffer values. The MELTS calculations stopped at ~90 to 93% crystallization, at which point the $SiO_2$ contents of the remaining melt had reached ~68 and 73 wt% for the tholeiitic and calc-alkaline series, respectively. Model outputs with associated isotopic mass-balance calculations are provided in the main text as well as supplementary online materials.

The fractionation factors between the minerals and melt were calculated at each step using the modeled *ab initio* force constants for the melt (see Sect. 2.4 for the 3 coordination models considered for the melt), the mean force constants for the minerals, and the temperature (in Kelvin) at each step in the crystallization process. The fractionation between the two phases, melt and minerals, were calculated using the following equation:

$$\Delta^{49}\mathrm{Ti}_{\mathrm{melt-minerals}} = 1000\ln\beta_{\mathrm{melt}} - 1000\ln\beta_{\mathrm{mineral}} = 3815\frac{\langle F\rangle_{\mathrm{melt}} - \langle F\rangle_{\mathrm{mineral}}}{T^2} \quad \text{(eq. 5)}$$

The isotopic composition of the residual melt at each step during the fractional crystallization process was calculated using the following relationship,

$$\delta^{49}\mathrm{Ti}_{\mathrm{melt},i+1} = \delta^{49}\mathrm{Ti}_{\mathrm{melt},i} + \Delta^{49}\mathrm{Ti}_{\mathrm{melt-minerals},i}\left(\frac{f_{\mathrm{Ti},i}}{f_{\mathrm{Ti},i+1}} - 1\right), \text{(eq. 6)}$$

where $\delta^{49}\mathrm{Ti}_{\mathrm{melt},i}$ and $\delta^{49}\mathrm{Ti}_{\mathrm{melt},i+1}$ are the isotopic compositions of the melts at steps $i$ and $i+1$, $\Delta^{49}\mathrm{Ti}_{\mathrm{melt-minerals},i}$ is the equilibrium isotopic fractionation between melt and the minerals that have crystallized between $i$ and $i+1$, and $f_{\mathrm{Ti},i}$ and $f_{\mathrm{Ti},i+1}$ are the fractions of Ti remaining in the melt at steps $i$ and $i+1$. The isotopic composition of the instantaneous crystals that grew in equilibrium with the melt between steps $i$ and $i+1$ is simply,

$$\delta^{49}\mathrm{Ti}^{\mathrm{instantaneous}}_{\mathrm{minerals},i\rightarrow i+1} = \delta^{49}\mathrm{Ti}_{\mathrm{melt},i} - \Delta^{49}\mathrm{Ti}_{\mathrm{melt-minerals},i}\text{ , (eq. 7)}$$

and the isotopic composition of the cumulative batch of minerals that have crystallized up to step $i$ can be readily calculated by mass-balance from the isotopic compositions of the melt and initial bulk $\delta^{49}\mathrm{Ti}_0$,

$$\delta^{49}\mathrm{Ti}^{\mathrm{cumulative}}_{\mathrm{minerals},i} = \frac{\delta^{49}\mathrm{Ti}_0 - f_{\mathrm{Ti},i}\delta^{49}\mathrm{Ti}_{\mathrm{melt},i}}{1-f_{\mathrm{Ti},i}}. \text{ (eq. 8)}$$

We use the Rhyolite MELTS [55, 56] program to calculate $f_{\mathrm{Ti}}$ at each temperature decrement (and crystallization increment). Based on our estimates of the equilibrium fractionation factors of Ti between minerals and melts ($\Delta^{49}\mathrm{Ti}_{\mathrm{melt-minerals}}$) as a function of temperature, melt composition, and nature of the minerals that crystallize (Sect. 3.1), we can calculate the isotopic composition of the magma, as well as instantaneous and cumulative solids during fractional crystallization.

## 3. Results and Discussion

### 3.1 Titanium-bearing mineral force constants and isotopic fractionation factors

Because we are primarily interested in high-temperature applications, we focus on the first order term in the polynomial expansion of the reduced partition function ratio (Eq. 3;

the coefficients of that expansion are compiled in Table 2), which is proportional to the mean force constant of the Ti bonds calculated by taking the second moment of the phonon density of states (Eq. 4) [36]. We provide in the Supplementary Online Materials the PDOS of Ti. Force constants were obtained for barium orthotitanate, fresnoite, potassium titanate, Ti-diopside, geikielite, karrooite, titanite, anatase, pseudobrookite, and $Ti^{3+}$ titanium oxide, respectively (force constants listed in Table 2). The relationship between the force constants calculated in this study and the inverse of the cube of the bond length (the ionic bond model predicts a linear relationship between $\langle F \rangle$ and $1/r^3$) [57, 58] together with reported literature values is shown in Fig. 3. A correlation between the two variables and the coordination environment of Ti (with the exception of one outlier) is observed. Greber *et al.* [59] found a similar correlation from literature data, but our new force constant calculations shows that it extends to more minerals. The inter-mineral Ti isotope fractionation factors are plotted in Fig. 4, and the Ti isotope β-factors and the fractionation factor between minerals and 5-fold coordinated fresnoite (a melt-proxy) are plotted as a function of temperature in Fig. 5. We did not calculate the silicate melts directly due to the difficulty in modeling disordered structure, but as discussed in Sect. 2.4, previous studies have shown that Ti in silicate melts comprises a significant fraction of Ti in 5-fold square pyramidal coordination [25, 31] as is encountered in fresnoite, which we take as a model mineral for this titanyl coordination. In mafic magmas, a significant fraction of Ti could be in 6-fold coordination, while in felsic magmas, a significant fraction could be in 4-fold coordination [25]. There are however many complications as other parameters such as the nature and abundance of network modifiers (e.g., Na, K, and Ca) can affect Ti coordination [25], but their roles have not been elucidated. More work is needed to characterize Ti-coordination in silicate melts of geological relevance. The coordination of Ti in most natural Ti-bearing minerals is 6-fold. Expectedly, we find that the strength of Ti bonds decreases with increasing coordination number from 4 to 6 (Fig. 3a). Given that silicate melts have lower coordination than minerals, we expect minerals to have light Ti isotopic compositions relative to melts, consistent with the view that coordination is likely the main driver of Ti isotopic fractionation during magmatic differentiation[6,11].

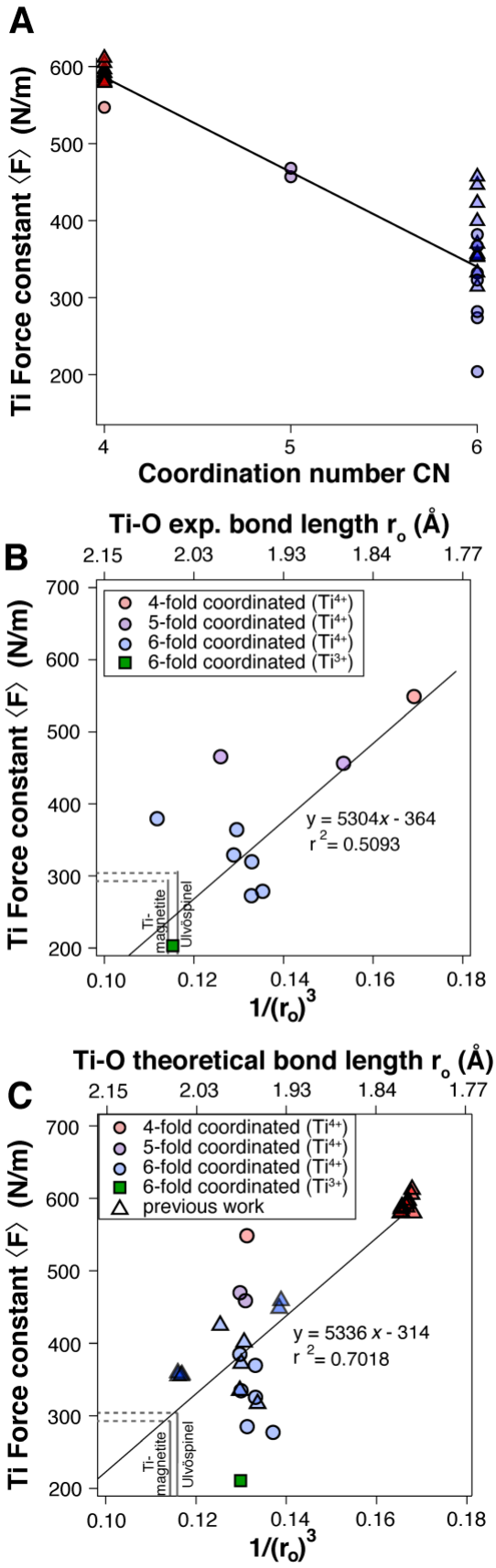
A
Ti Force constant ⟨F⟩ (N/m)
600
500
400
300
200
4
5
6
Coordination number CN
Ti-O exp. bond length r_o (Å)
B
2.15
2.03
1.93
1.84
1.77
700
600
500
400
300
200
4-fold coordinated (Ti4+)
5-fold coordinated (Ti4+)
6-fold coordinated (Ti4+)
6-fold coordinated (Ti3+)
y = 5304x - 364
r 2= 0.5093
Ti-magnetite
Ulvöspinel
0.10
0.12
0.14
0.16
0.18
1/(r_o)^3
Ti-O theoretical bond length r_o (Å)
C
previous work
y = 5336 x - 314
r 2= 0.7018

**Figure 3**. Influence of coordination environment on Ti bond strength. (A) Ti mean force constants (N/m) with respect to coordination number (CN) of Ti-bearing minerals investigated in this study (circles) and previous work (triangles) [30]. Minerals are color coded based on CN. Ti in lower CN forms stiffer bonds. (B) Ti experimental force constants (N/m) calculated in this study as a function of the inverse of the cube of the reported Ti-O bond length (Å) from literature data [26, 44, 60-67], color coded based on CN. (C) Ti mean theoretical force constants (N/m) as a function of the inverse of the cube of the reported theoretical Ti-O bond length (Å) from the literature[30] and this study color coded based on CN. We use the relationship between experimental bond length and force constant (B) to infer the force constants of the minerals that we are not able to calculate using DFT.

Wang *et al.* [30] also reported force constant determinations for Ti bearing phases. Focusing on $Ti^{4+}$-bearing minerals, they reported calculations for several silicates (clinopyroxene, orthopyroxene, olivine, pyrope) with $Ti^{4+}$ substituting for $Si^{4+}$ in 4-fold coordination as well as Ti in oxides, namely geikielite, ilmenite, and rutile where Ti is in 6-fold coordination. They further investigated how Ti dilution affected the force constant by using a supercell approach whereby only a fraction of the Si atoms was replaced by Ti. They found that dilution had little influence on the strength of the Ti bonds. There is overall good agreement between our calculations and the results of Wang *et al.* [30], in that Ti coordination seems to have a strong control on the strength of the Ti bonds (Fig. 3). In Fig. 3, 6-fold coordinated Ti in $Ti_2O_3$ using a different symbol as in this mineral, Ti is present as $Ti^{3+}$ whereas in all other minerals Ti is present as $Ti^{4+}$, which is relevant to redox conditions encountered on Earth.

The average force constant of Ti bonds in our *ab initio* calculations for $Ti^{4+}$ in 4-, 5-, and 6-fold coordination are 547, 462, and 327 N/m, respectively (Table 2). The average force constants of Ti bonds in Wang *et al.* [30] for $Ti^{4+}$ in 4- and 6-fold coordination are 590 and 378 N/m, respectively. For geikielite, Wang *et al.* [30] find a force constant of 399 N/m, which is slightly higher than the force constant in ilmenite of 332 N/m that they also calculate. For comparison, we calculate a force constant for geikielite of 367 N/m. It is

important to note that Wang *et al.* [30] and Leitzke *et al.* [31] use the LDA functional whereas this study uses the GGA (PBE) functional, resulting in systematically longer bond lengths and lower calculated force constants in this study (by approximately 30 N/m). The different approach means that there will not be a unique fit in Figure 3a, 3c, and 3d from the LDA and GGA dataset. We use the relationship between experimental bond lengths and theoretical force constants in order to estimate the force constants of the minerals that we were unable to model from their bond lengths. A shorter bond length generally corresponds to a higher force constant (Fig. 3b; e.g., stronger bond). A linear fit to the data $\langle F \rangle = 5336/r^3 - 314$; where $r$ is the average Ti-O bond length in Å; allows estimates on the force constants of Ti-bearing minerals that could not be modeled using DFT (Ti-magnetite and ulvöspinel). The average bond lengths of these two minerals are 2.06 and 2.046 Å [65] respectively, corresponding to calculated force constants of 296 and 309 N/m. This relationship between Ti force constant and coordination number can be fit with a function $\langle F \rangle = -123 \times \mathrm{CN} + 1078$ (note that 7-fold coordinated $Ti^{3+}$ was not included in this fit of $Ti^{4+}$-bearing minerals).

Titanium isotopic compositions of mineral separates from different rocks crystallizing at various temperatures [59, 68] allows for the comparison of our modeled Ti force constants with natural samples. In the Kneeling Nun Tuff that crystallized at ~700 ± 30 °C, Mandl [68] reports $\Delta^{49}$Ti values between titanite-magnetite, ilmenite-magnetite, quartz-magnetite, and plagioclase-magnetite of +0.23, +0.10, +1.12, and +0.98‰ (all ± 0.04‰), respectively. In the Kos magmatic suite from the Aegean arc, differences in the $\delta^{49}$Ti measured compositions for quartz-magnetite (equilibrated at ~700°C), plagioclase-magnetite (equilibrated at ~770°C) and olivine-magnetite (equilibrated at ~1150°C) ranged from +1.08 , +0.77 and +0.43 ‰ (all samples ± 0.05‰)[59]. In synthetic minerals and glasses produced at various $fO_2$ glasses equilibrated at 1260°C (here reported at *f*O2=air), Rzehak *et al.*[69] reports $\Delta^{49}$Ti values between orthopyroxene-glass and armalcolite-glass of 0‰ and -0.09‰ (±0.01, 0.02, and 0.01‰ for orthopyroxene, armalcolite, and glass respectively). In Fig. 4, the measured differences in $\delta^{49}$Ti between the mineral separates [59, 68, 69] are compared to those predicted by our DFT calculations with the assumption that the Ti force constant of $Ba_2TiO_4$ is a good analogue for olivine,

plagioclase and quartz (in all phases Ti is incorporated in 4-fold coordination), and the melt for our predicted isotope fractionation is 40% [6] and 60% [5]. Although we did not model orthopyroxene and armalcolite here, we compare these measured compositions[69] to our predicted isotope fractionations of clinopyroxene-melt, and several Ti-rich oxides modeled here: pseudobrookite-melt, geikielite-melt, and karrooite-melt. The modeled and measured inter-mineral $\delta^{49}$Ti differences agree to a first order, with the largest difference being that Mandl [68] found a heavier Ti isotopic fractionation between titanite-magnetite than in ilmenite-magnetite, which is not predicted by this study. It is important to mention that isotopic analyses of natural samples do not always record equilibrium isotope fractionation; for example, samples may be not be co-genetic or may have experienced Ti diffusion. Estimating precise equilibrium temperatures is difficult, and the measured $\delta^{49}$Ti composition of minerals with low Ti concentrations could be additionally biased by mineral and melt inclusions.

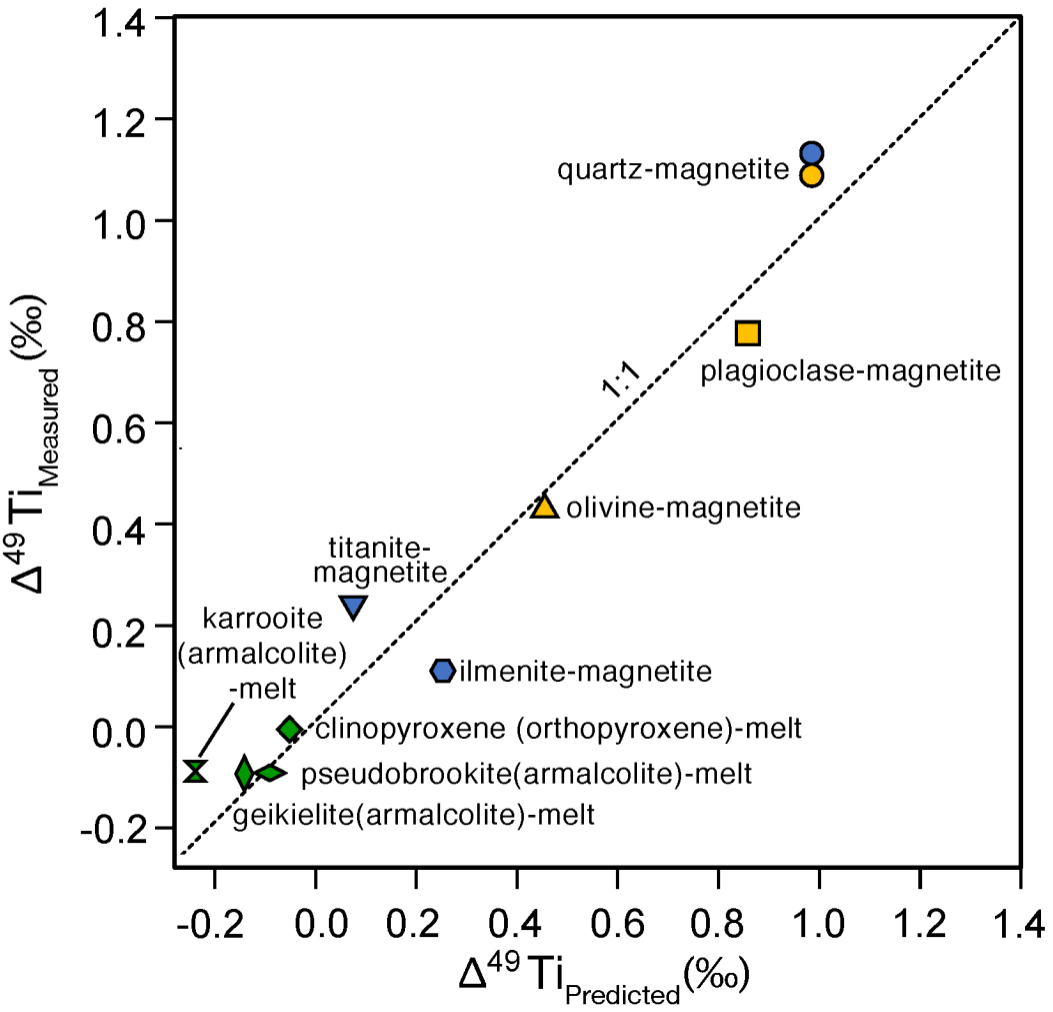


**Figure 4**. Relationship between measured [59, 68, 69] and predicted (this study) Ti isotopic compositions of mineral pairs. Blue symbols are $\Delta^{49}$Ti values from Kneeling Nun Tuff between titanite-magnetite, ilmenite-magnetite, plagioclase-magnetite, and quartz-magnetite [68]. Yellow symbols are $\Delta^{49}$Ti values from Kos magmatic suite between quartz-magnetite, plagioclase-magnetite and olivine-magnetite[59] (data from sample KS-041 is not shown as it likely does not record equilibrium conditions). Green symbols are $\Delta^{49}$Ti values from synthetic Ti oxides, silicates, and glasses. Shown here are orthopyroxene-glass and armalcolite-glass[69] compared to calculated clinopyroxene [30, 31], pseudobrookite (this study), and geikielite (this study) and the proxy for melt used in this study (40% [6]+60% [5]=423 N/m).

As discussed in Sect. 2.4, we consider three scenarios for the coordination of Ti in silicate melt. For 4-, 5-, and 6-fold coordinated Ti in silicate melt, we adopt the following force constants of Ti: (1) The 4-fold coordinated Ti is the average value of the only 4-fold coordinated mineral that we studied ($Ba_2Ti^{4+}O_4$; 547 N/m; Table 2) and the average of force constants calculated by Wang *et al.*[30,] (592 N/m) and those calculated for minerals discussed by Leitzke *et al.*[31] for $Ti^{4+}$ in 4-fold coordination (633 N/m; based on the relationship defined here between coordination number and force constant). (2) The 5-fold coordinated Ti is the value of fresnoite calculated here (Table 2; 468 N/m), which hosts Ti in a coordination that resembles that encountered in silicate glasses [25]. (3) The 6-fold coordinated is the average value of 6-fold coordinated minerals investigated here (327 N/m; Ti-diopside; 383 N/m, geikielite; 367 N/m, karrooite; 335 N/m, titanite; 323 N/m, pseudobrookite; 274 N/m, anatase; 282 N/m), and the 6-fold coordinated values of Leitzke *et al.* [31] and Wang *et al.* [30] for clinopyroxene (426 N/m [20] and 354 N/m [30]), orthopyroxene (353 N/m[30]), pyrope (445 N/m [30]), geikielite (399 N/m [30]), ilmenite (332 N/m [30]), and rutile (314 N/m [30]). There are significant variations in the force constant of 6-fold coordinated Ti in minerals likely due to the different approaches (GGA versus LDA), but given that this coordination is a minor component of Ti in silicate melt, this uncertainty has little influence on the conclusions of this study.

For the three Ti-coordination models of silicate melt introduced in Sect. 2.4, we therefore use the following force constants:

(1) 100% [5] = 468 N/m.
(2) 40% [6]+60% [5]=423 N/m for <52wt% $SiO_2$; 100% [5]=468 N/m for 52-63 wt% $SiO_2$, and 45% [4]+55%[5]=523 N/m for >63 wt% $SiO_2$.
(3) $\langle F \rangle_{melt} = -60 \times \mathrm{NBO/T} + 463$. To relate force constant to melt polymerization, we use the gross correlation between force constant and coordination number (Fig. 3a; $\langle F \rangle_{melt} = -123.5 \times \mathrm{CN} + 1078$) and use the correlation of Ti coordination with NBO/T in the data of Farges and Brown [25] (Fig. 2b; $\mathrm{CN} = 0.485 \times \mathrm{NBO/T} + 5$).

To test the validity of the Ti force constants adopted here for the melt, we compare our predictions with measured Ti isotopic fractionation in mineral-melt pairs from natural samples. Mineral separates from Kīlauea Iki lava lake gave a fractionation of $\Delta^{49}Ti_{melt\text{-}oxide} = +0.39 \pm 0.06$‰ at 1000 °C [11]. Using the estimate of the coordination environment of Ti in basalt (BCR-2: 50% 5-fold coordinated, 50% 6-fold coordinated) from [25], the force constant of the melt should be $\langle F \rangle$ = 370 N/m. To achieve a +0.39 ‰ $\delta^{49}$Ti isotopic fractionation at 1000 °C would require a force constant of Ti in minerals (in this case a mixture of ilmenite and Ti-magnetite) of 204 N/m. This force constant is significantly lower than the *ab initio* derived $\langle F \rangle$ value for Ti in 6-fold coordinated minerals of 327 N/m (this study) or the value of 332 N/m calculated for ilmenite by Wang *et al.* [30]. The reason for this discrepancy is unclear but could be attributed to differences in the coordination and force constant of Ti in silicate melts. For example, if we assume that Ti in the melt is in 5-fold coordination and has a force constant of 468 N/m, then the force constant of the minerals required to explain the results of Johnson *et al.* [11] becomes 302 N/m, which is more in line with our prediction for 6-fold coordinated minerals (327 N/m). Alternatively, the force constant of ilmenite could be lower than the value of other 6-fold coordinated minerals, as it has among the lowest force constants (332 N/m) for all 6-fold coordinated minerals (range from 314-457 N/m) calculated by Wang *et al.* [30]. Measurements of the bulk mineralogical composition using SEM-EDX of four samples from Kīlauea Iki heavy mineral separates containing oxides indicate that the average abundance of Ti partitioned into ilmenite versus Ti-magnetite is 67.75 and 32.25%, respectively (see Supplementary Online material). The estimated amount of Ti in each mineral phase along with the *ab initio* derived $\langle F \rangle$ value of ilmenite from Wang *et al.* [30] allows us to calculate an $\langle F \rangle$ value of 238 N/m between Ti-magnetite and a 5-fold coordinated melt. For the model presented here, we use a range of different conditions to account for uncertainties. However it is clear that more work is needed to quantify Ti isotopic fractionation in more mineral-melt pairs and to better constrain the coordination of Ti in geologically relevant melts.

| | | *a* (Å) | *b* (Å) | *c* (Å) | *α* (°) | *β* (°) | *γ* (°) |
|---|---|---|---|---|---|---|---|
| | Cal. | 6.212 | 7.725 | 11.951 | 90 | 117.44 | 90.01 |

| | | | | | | | |
|---|---|---|---|---|---|---|---|
| Barium orthotitanate $Ba_2Ti^{4+}O_4$ | Exp. | 6.12 | 7.7 | 11.861 | 90 | 117.88 | 90 |
| Potassium titanite $K_2Ti^{4+}{}_2O_5$ | Cal. | 6.045 | 6.045 | 6.702 | 98.93 | 98.93 | 36.78 |
| | Exp. | 5.994 | 5.994 | 6.62 | 99.57 | 99.57 | 36.96 |
| Fresnoite $Ba_2Ti^{4+}Si_2O_8$ | Cal. | 8.618 | 5.297 | 5.376 | 90 | 90 | 90 |
| | Exp. | 8.518 | 5.211 | 5.366 | 90 | 90 | 90 |
| Ti-Diopside $Ti^{4+}Si_2O_6$ | Cal. | 6.576 | 6.576 | 5.526 | 75.303 | 75.303 | 84.280 |
| | Exp. | 6.582 | 6.582 | 5.477 | 75.211 | 75.211 | 84.336 |
| Geikielite $MgTi^{4+}O_3$ | Cal. | 5.526 | 5.526 | 9.451 | 54.92 | 54.92 | 54.92 |
| | Exp. | 5.477 | 5.477 | 10.129 | 54.98 | 54.98 | 54.98 |
| Karrooite $MgTi^{4+}{}_2O_5$ | Cal. | 5.251 | 5.251 | 10.118 | 90 | 90 | 41.896 |
| | Exp. | 5.204 | 5.204 | 10.129 | 90 | 90 | 42.080 |
| Titanite $CaTi^{4+}SiO_5$ | Cal. | 7.132 | 8.763 | 10.052 | 90 | 90 | 114.1 |
| | Exp. | 7.068 | 8.714 | 9.93 | 90 | 90 | 113.82 |
| Pseudobrookite $Fe^{3+}{}_2Ti^{4+}O_5$ | Cal. | 5.321 | 5.321 | 10.052 | 90 | 90 | 41.39 |
| | Exp. | 5.237 | 5.237 | 9.93 | 90 | 90 | 41.463 |
| Anatase $Ti^{4+}O_2$ | Cal. | 3..7845 | 3.7845 | 3.7845 | 90 | 90 | 90 |
| | Exp. | 3.785 | 3.785 | 3.785 | 90 | 90 | 90 |
| Titanium oxide $Ti^{3+}{}_2O_3$ | Cal. | 5.521 | 5.521 | 5.521 | 55.012 | 55.012 | 55.012 |
| | Exp. | 5.433 | 5.433 | 5.433 | 56.573 | 56.573 | 56.573 |

**Table 1.** Calculated (cal.) and experimental (exp.) [38-46] crystal lattice parameters of minerals studied here.

| Ti isotope β-factors at 1200 K, and Ti coordination number for Ti-bearing minerals[a] | | | | Polynomial expansion coefficients[b] | | |
|---|---|---|---|---|---|---|
| | $\langle F \rangle$ (N/m) | $1000\ln\beta^a$ | CN | $A_1$ | $A_2$ | $A_3$ |
| Barium orthotitanate $Ba_2Ti^{4+}O_4$ | 547 | 1.45 | 4 | $2.14\times10^6$ | $2.93\times10^{10}$ | $6.56\times10^{14}$ |
| Potassium titanite $K_2Ti^{4+}{}_2O_5$ | 457 | 1.21 | 5 | $1.78\times10^6$ | $2.41\times10^{10}$ | $6.62\times10^{14}$ |
| Fresnoite $Ba_2Ti^{4+}Si_2O_8$ | 468 | 1.23 | 5 | $1.82\times10^6$ | $2.873\times10^{10}$ | $8.57\times10^{14}$ |
| Ti-Diopside $Ti^{4+}Si_2O_6$ | 383 | 1.01 | 6 | $1.49\times10^6$ | $1.62\times10^{10}$ | $4.28\times10^{14}$ |
| Geikielite $MgTi^{4+}O_3$ | 367 | 0.97 | 6 | $1.43\times10^6$ | $1.40\times10^{10}$ | $2.71\times10^{14}$ |
| Karrooite $MgTi^{4+}{}_2O_5$ | 335 | 0.89 | 6 | $1.31\times10^6$ | $1.24\times10^{10}$ | $2.56\times10^{14}$ |
| Titanite $CaTi^{4+}SiO_5$ | 323 | 0.86 | 6 | $1.26\times10^6$ | $1.15\times10^{10}$ | $2.54\times10^{14}$ |
| Pseudobrookite $Fe^{3+}{}_2Ti^{4+}O_5$ | 274 | 0.73 | 6 | $1.10\times10^6$ | $8.10\times10^9$ | $1.52\times10^{14}$ |

| | | | | | | |
|---|---|---|---|---|---|---|
| Anatase $Ti^{4+}O_2$ | 282 | 0.75 | 6 | $1.16\times10^{6}$ | $1.06\times10^{10}$ | $2.76\times10^{14}$ |
| Titanium oxide $Ti^{3+}{}_2O_3$ | 204 | 0.54 | 6 | $7.98\times10^{5}$ | $3.21\times10^{9}$ | $2.46\times10^{13}$ |

**Table 2.** Calculated force constants, isotope fractionation factors, and parameters of Ti-bearing minerals from this study. [a]Ti isotope β-factors at 1200 K, and Ti coordination number for Ti-bearing minerals. The PDOS for Ti and other structural elements are given in Supplementary Online Materials. [b]The polynomial expansion equation is: $10^3 \ln \beta = A_1/T^2 + A_2/T^4 + A_3/T^6$.

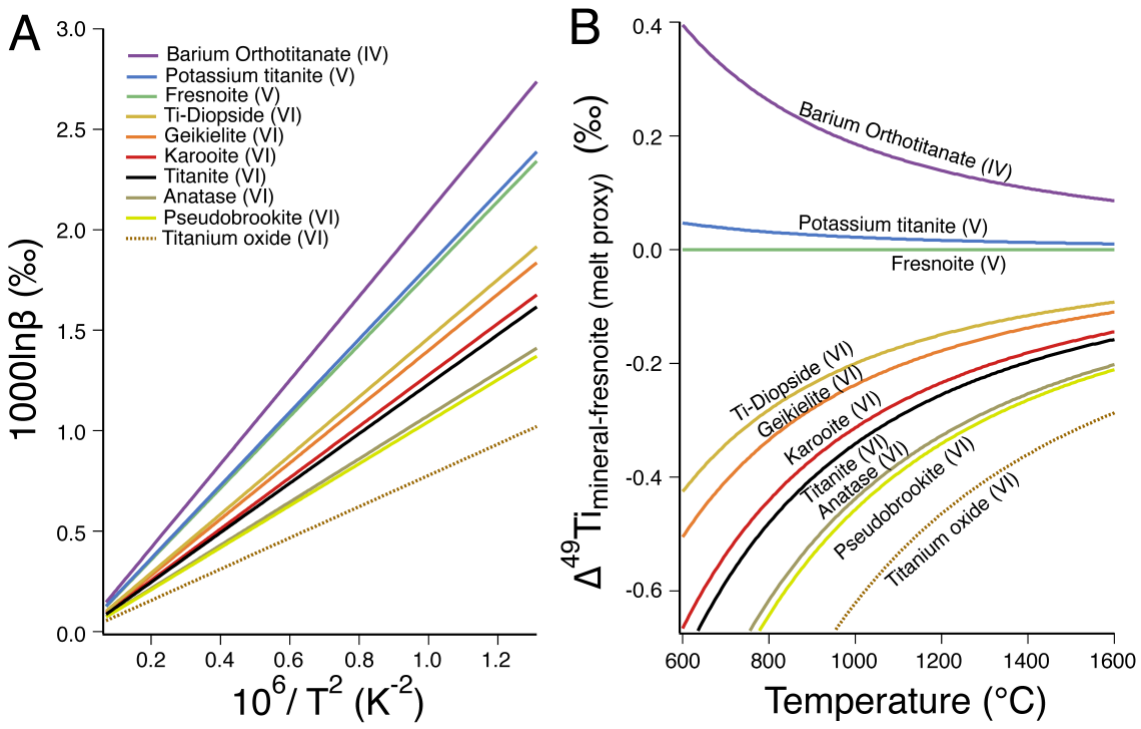


**Figure 5**. (A) $^{49}Ti/^{47}Ti$ isotope β-factors of Ti-bearing minerals as a function of temperature (using Eq. 4 and the coefficients compiled in Table 2). (B) Equilibrium isotopic fractionation factor between various minerals and fresnoite (mineral proxy for 5-fold coordinated Ti in silicate melt) as a function of temperature calculated using DFT. All the minerals contain $Ti^{4+}$ except titanium oxide, which contains $Ti^{3+}$ and is therefore depicted using a dashed line.

### 3.2 MELTS Modeling: Ti isotopic fractionation during magmatic differentiation

We modeled the fractional crystallization and the corresponding Ti isotopic fractionation of tholeiitic and calc-alkaline basalts using Rhyolite MELTS [55, 56] and the equilibrium isotopic fractionation factors that we derived (Sect. 2.5, 3.1, Fig. 5). For specific details on the initial conditions see Figure captions 6 and 7.

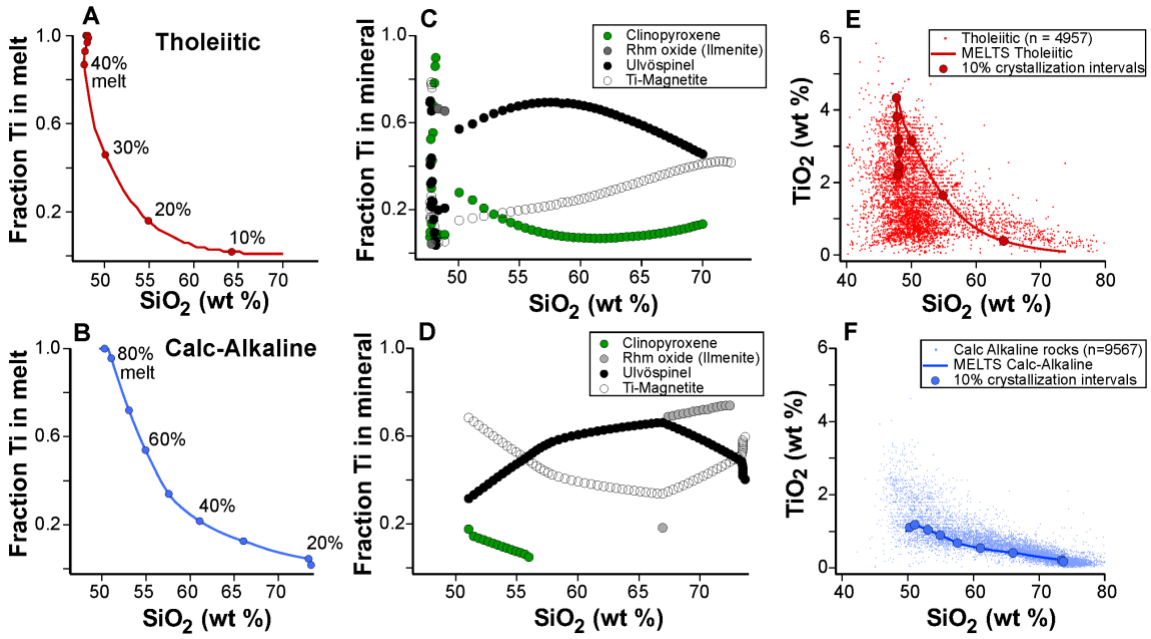


**Figure 6.** Titanium distribution during fractional crystallization of tholeiitic (top panels) and calc-alkaline (bottom panels) series magmas. The top panels correspond to fractional crystallization of a tholeiitic basalt (starting composition in wt %: $SiO_2$=47.8, $TiO_2$=2, $Al_2O_3$=17.3, $Fe_2O_3$=1.2, FeO= 7.6, $Cr_2O_3$=0.04, MgO=9.0, $Na_2O$=2.6, $K_2O$=0.02, $P_2O_5$=0.07) with a starting $fO_2$ of ΔQFM=-0.3 and $H_2O$ content of 0.2 wt% (the $fO_2$ is not buffered). The bottom panels correspond to fractional crystallization of a calc-alkaline basalt (starting composition in wt %: $SiO_2$=50, $TiO_2$=1, $Al_2O_3$=18.4, $Fe_2O_3$=2.1, FeO=9.0, $Cr_2O_3$=0.0, MgO=5.5, $Na_2O$=2.5, $K_2O$=0.7, $P_2O_5$=0.2) with a starting $fO_2$ of ΔQFM=+0.6 and $H_2O$ content of 1.8 wt% (the $fO_2$ is not buffered). The Rhyolite-MELTS software was used to model these evolutions. (A, B) Changes in the fraction of Ti in the melt and the percentage of minerals crystallized during fractional crystallization of tholeiitic and calc-alkaline rocks. Percent of melt remaining as a function of $SiO_2$ content during fractional crystallization are given in 10% intervals. (C, D) Fraction of titanium removed from melt into crystallizing minerals during an increment of crystallization in tholeiitic and calc-alkaline magma as a function of $SiO_2$; where 1 indicates the total Ti removal from the melt during an increment of crystallization. (E, F) Comparison between the modeled $TiO_2$ concentration trends in residual melt (solid lines) during fractional crystallization of tholeiitic and calc-alkaline magma and literature rock data (small red and blue dots) from a database [70]. Percentages of melt crystallized are also plotted as red and blue filled circles.

The Ti isotopic compositions of melts and minerals during magmatic differentiation were modeled using the abundances of the minerals crystallizing at each stage, the melt fraction, the corresponding Ti concentrations, and the Ti mean force constants derived from *ab initio* calculations and empirical relationships between bond strength and interatomic distance (Sect. 3.1). For both the tholeiitic and calc-alkaline melts, the primary Ti-bearing mineral phases were solid solutions of clinopyroxene ($CaTi_{0.5}Mg_{0.5}AlSiO_6$, $CaTi_{0.5}Mg_{0.5}Fe^{3+}SiO_6$), spinel (Ti-magnetite: $Fe^{2+}(Fe^{3+},Ti)_2O_4$ and ulvöspinel: $TiFe^{2+}{}_2O_4$), and rhombohedral oxide (primarily ilmenite: $Fe^{2+}TiO_3$). The proportions of these Ti-bearing mineral phases were monitored throughout the course of the crystallization (Fig. 7), and the force constants of the minerals were weighted based on the mineral proportions and Ti contents. The Ti force constants adopted in the modeling for clinopyroxene, spinel, and rhombohedral oxide are:

(i) Under reducing conditions (~IW-1.7) and with large amounts of Ti, Leitzke *et al.* [31] found based on XANES measurements of experimental run products that clinopyroxene consisted of a 50-50 mixture of 4- and 6-fold coordinated Ti [31] . In Ti-rich natural terrestrial diopside, Quartieri *et al.* [71] found that Ti coordination ranged from mostly 4-fold to a mixture of 4- and 6-fold sites. The coordination of Ti in clinopyroxene compositions more relevant to the magmatic differentiation series studied here is uncertain but as a first pass on this estimate, we will assume that it is a 50%-50% mixture of 4 and 6. Wang *et al.* [30]and Leitzke *et al.* [31] calculated the force constant of $Ti^{4+}$ in 4-fold coordination substituting for Si and obtained values of 592 and 633 N/m, respectively. For Ti in 4-fold coordination in barium orthotitanite, we calculate a force constant of 547 N/m. Leitzke *et al.* [31] calculated the force constant of $Ti^{4+}$ in 6-fold coordination substituting for Mg in clinopyroxene and obtained a value of 350 N/m. Our calculation for Ti in 6-fold coordination in Ti-diopside gives a value of 383 N/m. Taking all 4-fold (orthotitanate in Table 2, Si-substituted from Wang *et al.* [30] and Leitzke *et al.* [31]) and 6-fold values (Ti-diopside in Table 2, Mg-substituted from Leitzke *et al.* [31]), we obtain averages of 591 and 366 N/m, which corresponds to a clinopyroxene value of ~478 N/m for a 50%-50% mixture of 4- and 6-fold coordination. Due to large uncertainties in Ti coordination in clinopyroxene, this value is uncertain but given that

clinopyroxene plays a secondary role in the budget of Ti in tholeiitic and calc-alkaline series, this has little impact on the conclusions.

(ii) Ti-magnetite $Fe_{3-x}Ti_xO_4$ forms a solid solution between magnetite and ulvöspinel. For 4-oxygens, there are 3 cation sites: 1 tetrahedral A-site and 2 octahedral B-sites. In magnetite, the tetrahedral A-site is occupied by $Fe^{3+}$ while the 2 B-sites are occupied by $Fe^{3+}$+$Fe^{2+}$. $Ti^{4+}$ substitution is thought to be achieved by replacement of $Fe^{3+}$ in the B-site and conversion of $Fe^{3+}$ to $Fe^{2+}$ to respect charge-balance. According to this view, $Ti^{4+}$ is thought to be predominantly in 6-fold coordination, which is supported by several observations [72-75]. Hoare *et al.* [12] recently argued for the presence of large amounts of Ti in 4-fold coordination in Ti-magnetite based on data subsequently disputed in a study by Wechsler *et al.* [73]. As discussed in Sect. 2.4, we were unable to properly calculate the force constant of Ti in ulvöspinel and Ti-magnetite because the structures calculated by DFT were dynamically unstable and produced negative frequencies. For ulvöspinel, we used the primitive cell (space group Fd-3m) with an antiferromagnetic ordering. Optimized cell parameters show an agreement with experimental values [76] similar as for other minerals, with a slight distortion of cell. Two negative frequencies out of the center of the Brillouin zone are obtained, even if the structural relaxation is constrained to the cubic cell. By neglecting these imaginary modes, we found a Ti force constant of 155 N/m. For Ti-magnetite, we also used the primitive cell (space group Fd-3m) and built a ferrimagnetic structure with the same charge ordering as in the theoretical work of Liu and Di Valentin [77] for pure magnetite. By neglecting the imaginary frequency displayed out of the center of the Brillouin zone, we found a Ti force constant of 145 N/m. DFT+U (the on-site Coulomb term U) method is often used for improving the description of the electronic structure of Fe-bearing minerals like magnetite, but this improvement is often obtained at the expense of the structural properties. Obtaining the PDOS from the vibrational frequencies calculated in DFT+U on a q-point grid requires large computational resources. Several attempts were performed here but results were not conclusive and seem very dependent on the pseudopotentials used. Therefore, to estimate the force constant of Ti in Ti-magnetite and ulvöspinel, we use the relationship between the inverse of the cube of the reported bond lengths and force constants of Ti-bearing

minerals illustrated in Fig. 3, which correspond to calculated force constants of 296 and 309 N/m for Ti-magnetite and ulvöspinel respectively.

Oxygen fugacity will have an influence on type and abundance of crystallizing minerals (e.g., in Rhyolite MELTS the proportion of rhm oxide or ilmenite to spinel) as well as the partitioning of $Fe^{3+}$ versus $Fe^{2+}$ partitioned into various mineral phases. Because the force constant of spinel (and therefore the average of crystallizing minerals) could be affected by the spinel stoichiometry on the magnetite-ulvöspinel solid solution, and in particular the proportion of $Fe^{3+}$, we express it as a linear function of the molar ratio $x = Fe^{3+}/(Fe^{2+} + Fe^{3+})$: $\langle F \rangle_{\text{Spinel}} = \frac{3x}{2}\langle F \rangle_1 + (1 - \frac{3x}{2})\langle F \rangle_2$, where $\langle F \rangle_1$ and $\langle F \rangle_2$ are the estimated force constants that would correspond to the force constants of Ti-bonds in Ti-magnetite and ulvöspinel, respectively. In the Rhyolite MELTS calculation, $x$ varies between 0.23 and 0.46 in the tholeiitic series, and 0.3 to 0.54 in the calc-alkaline series, which is far from the pure end-member compositions.

(iii) Similar to Ti-magnetite and ulvöspinel, DFT modeling of ilmenite is complicated by the fact that it contains Fe. Therefore, we have instead modeled geikielite ($MgTiO_3$), which is a rhombohedral titanate with the same crystal structure as ilmenite and contains Ti in 6-fold coordination [44]. The mean force constant of Ti that we calculate for geikielite is 367 N/m. This value is in line with the results of Wang *et al.* [30] , who calculated the force constant of Ti in the geikielite-ilmenite solid solution and obtained values of 399 N/m, for 100% Mg, 370 N/m for 50% Mg-50% Fe, and 332 N/m for 100% Fe. Here we average the force constant of geikielite (367 N/m; this study) and 100% Fe ilmenite (332 N/m; Wang *et al.* [30]) to obtain 350 N/m for rhm oxides modeled in the Rhyolite MELTS calculation.

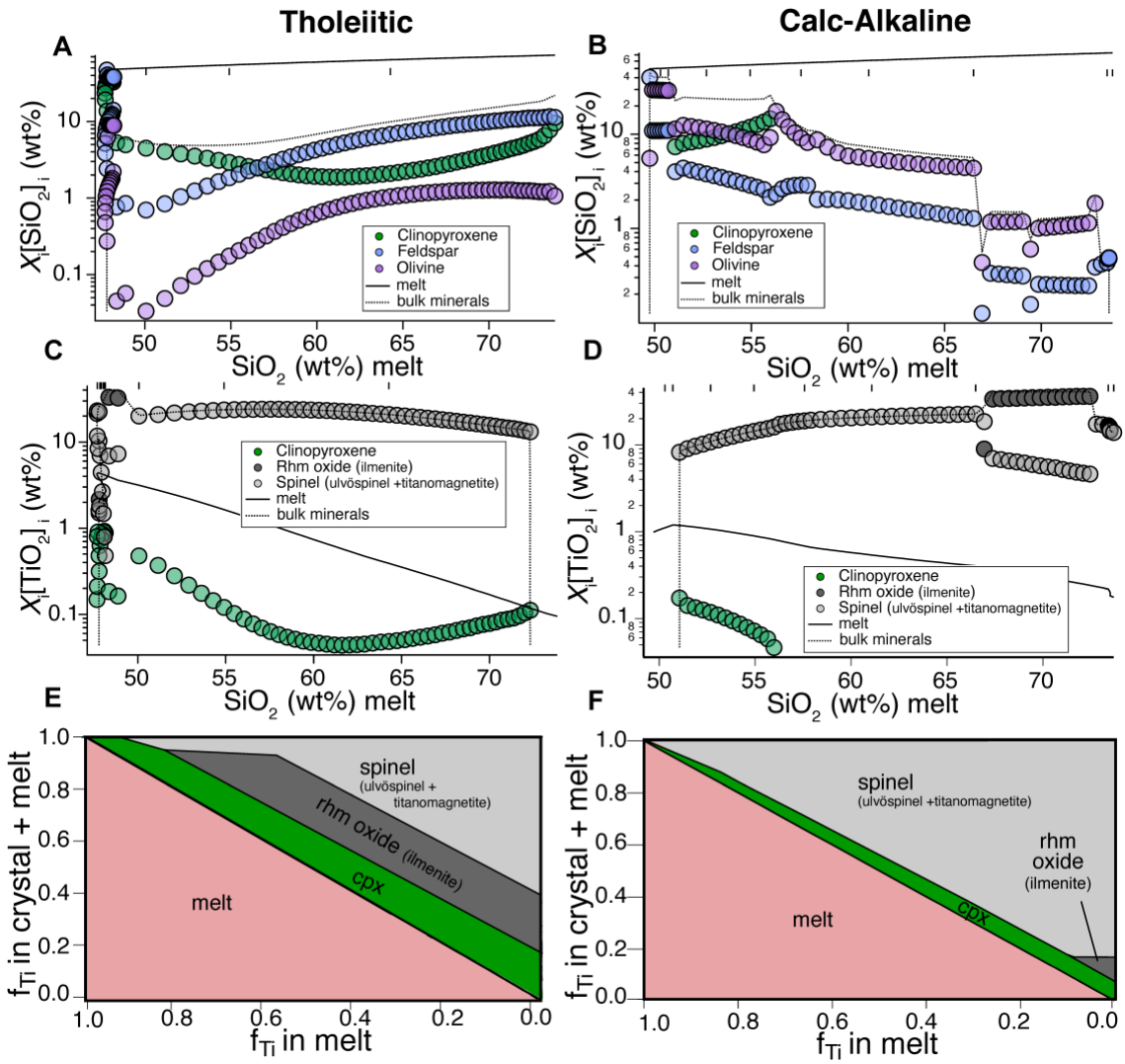


**Figure 7.** $SiO_2$ and $TiO_2$ behaviors during fractional crystallization of tholeiitic (left panels) and calc-alkaline (right panels) series magmas (see Figure 6 caption for initial melt compositions and conditions). The Rhyolite-MELTS software was used to model these evolutions. (A, B) Comparison of mass fraction weighted $SiO_2$ content of individual minerals and total bulk mineral $SiO_2$ content (where $X$ is the mass fraction of mineral, $i$ is the mineral of interest, and $[SiO_2]_{bulk\ minerals} = \sum_i X_i[SiO_2]_i$) as a function of $SiO_2$ content of the melt during fractional crystallization. The total fraction of the mineral assemblage is multiplied by the $SiO_2$ weight percent of the mineral phase at each step of the fractional crystallization process. The high modal fraction of feldspar in the tholeiitic series mitigates the rise of $SiO_2$ in the melt during magmatic differentiation of tholeiitic magma. (C, D) The black solid and dashed curves are the $TiO_2$ concentrations of the melt and bulk mineral assemblages, respectively. Bulk minerals plotting above the melt line are driving the $TiO_2$ content of the melt to lower concentrations and vice versa. (E, F) Cumulative fractions of Ti in Ti-bearing minerals and the melt as a function of the fraction of Ti in the melt during fractional crystallization (see [78] for a similar figure applied to Zr). Tick marks on top in panels A, B, C, and D represent increments of mineral crystallization in 10% intervals.

### 3.3 Divergent Ti isotopic evolution in tholeiitic versus calc-alkaline magmas

Measurements of natural samples show that $\delta^{49}$Ti increases more steeply with $SiO_2$ content in the tholeiitic series than in the calc-alkaline series (Fig. 8) [6, 7, 9, 11]. This observation may seem counter intuitive as the onset of Fe-Ti oxide crystallization is delayed (with respect to fraction crystallized) in the tholeiitic series relative to the calc-alkaline series. The main reason for this apparent paradox is that plagioclase crystallization starts earlier in the tholeiitic series compared to the calc-alkaline series, and because plagioclase is rich in $SiO_2$, its early crystallization slows the enrichment of $SiO_2$ in the melt with fractional crystallization (Fig. 6a, b, Fig. 7a, b).

The two main uncertainties affecting the calculation of Ti isotopic fractionation during magmatic differentiation are the coordination of Ti in silicate melt (Sect. 2.4), and the force constant of Ti in the Ti-magnetite solid solution (Sect. 3.2). We set the force constants of ilmenite, clinopyroxene, and the Ti-magnetite solid solution to the values given in Sect. 3.2. In the melts, we consider three models for the coordination and force constant of Ti bonds (Sect. 2.4, 3.2): (*i*) we assume that Ti is solely 5-fold (Fig. 8a), (*ii*) we assume that it changes from a mixture of 6- and 5-fold in more mafic magmas, pure 5-fold in intermediate magmas, and a mixture of 5- and 4-fold in more felsic magmas (Fig. 8b), and (*iii*) we assume that it changes with the degree of polymerization of the melt quantified using the NBO/T ratio (Fig. 8c).

The $\delta^{49}$Ti values of both compositions remain close to the chondritic value of ~0‰ [10] until the onset of Ti-bearing mineral crystallization (Fig. 8). The Ti-bearing minerals such as clinopyroxene, ulvöspinel, Ti-magnetite, and geikielite incorporate light Ti isotopes, driving the residual melt to heavier compositions. Our MELTS model correctly predicts that tholeiitic magmas should produce a steeper trend in the Ti isotope versus $SiO_2$ space compared to calc-alkaline magmas, although the trends do not match exactly the observed values in natural samples. The two first melt-coordination models (Fig. 8a, b) highlighted above reproduce well tholeiitic series $\delta^{49}$Ti values, but we predict a steeper slope for calc-alkaline rocks than what is actually measured. The third melt-coordination scenario (Fig. 8c) based on NBO/T is very successful in reproducing the observed trend of tholeiitic magmas and best reproduces the calc-alkaline trend observed

in natural samples, although a large discrepancy remains for this magma series. The agreement between data and model (Fig. 8c) suggest that melt polymerization may have an important control on Ti isotopic composition, calling for further experimental validation. The reason for these models' remaining discrepancies is unknown and further work is needed to explore how water content, $fO_2$, pressure, temperature, and composition affect the coordination of Ti in calc-alkaline and tholeiitic magmas and crystallizing minerals. A possibility for the discrepancy between model predictions and measurements of natural samples could be due to the abundance and composition of Fe-Ti oxide crystallization during magmatic differentiation in the MELTS model [12.], as various Fe-bearing minerals can have unique $\langle F \rangle$ (Table 2) which translate to variable Ti isotopic fractionation factors. Furthermore, in calc-alkaline magmatic systems, amphibole and biotite are common silicate phases that can also contain a substantial amount of Ti. Measurement of amphibole and biotite mineral separates indicate that they do not fractionate Ti isotopes as strongly as Fe-Ti oxides, but likely also have lighter $\delta^{49}$Ti compositions than the corresponding melt [11, 59, 68]. While the Rhyolite-MELTS software predicts the evolution of the melt Ti concentration accurately during magmatic differentiation, it does not partition Ti into amphibole and biotite phases and thus likely overestimates the amount of crystallizing Fe-Ti oxides. The outcome of this would likely lead to a heavier modeled $\delta^{49}$Ti composition of the melt compared to reality. One other explanation for disagreement between our modeled calc-alkaline magmas and natural samples is the possibility of assimilation or magma mixing as discussed in Greber *et al.*[59].

To summarize, our work shows that Ti coordination has a major influence on Ti isotopic fractionation during magmatic differentiation and we can successfully reproduce the trend documented in tholeiitic rocks, but our model predicts a larger Ti isotopic fractionation in calc-alkaline rocks than what is measured. Once the controls on Ti isotopic fractionation are ascertained, this system can potentially be used to reconstruct the history of oxide crystallization of igneous rocks for which a full magmatic differentiation series is not available, and possibly tease out the effects of assimilation and magma mixing[5],57. It may also yield new insights into magma differentiation early in Earth's history [13] and compositions relevant to partial melting and differentiation in the Archean (*e.g.*, rutile, TTGs).

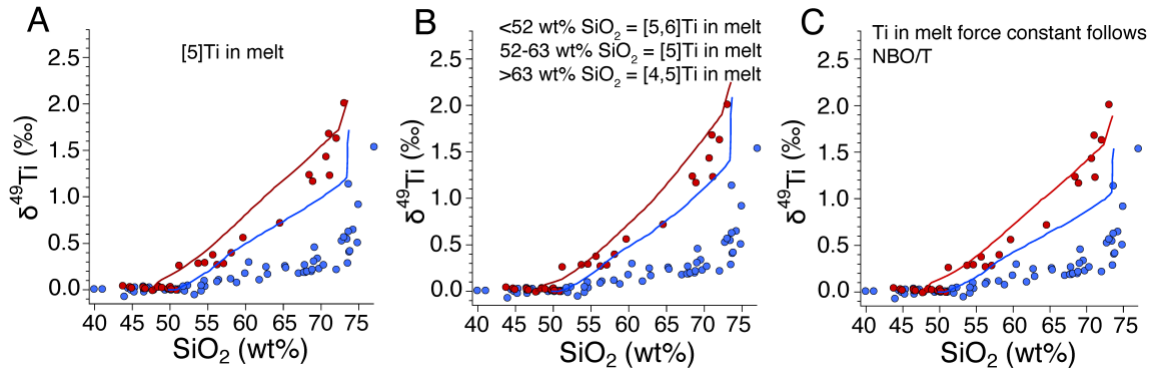


**Figure 8.** Titanium isotopic evolution of melt during magmatic differentiation of calc-alkaline (blue line) versus tholeiitic magma (red line) as modeled by changes in Ti concentration of the melt and the *ab initio* derived fractionation factors of the crystallizing phases. Existing literature Ti isotope data for tholeiitic rocks from Iceland and Hawaii [7, 11] (red circles) and diverse calc-alkaline rocks [6, 9] (blue circles) are plotted for comparison. (A) 100% 5-fold coordinated Ti in the melt, (B) evolving Ti coordination during magmatic differentiation: at <52 wt% $SiO_2$, 40% 6-fold and 60% 5-fold coordinated Ti in the melt, 52-63 wt% $SiO_2$, 100% 5-fold coordinated Ti in the melt, and >63 wt% $SiO_2$, 45% 4-fold and 55% 5-fold coordinated Ti in the melt, and (C) the force constant of the melt follows NBO/T. For the force constant of spinel (e.g., Ti-magnetite and ulvöspinel), we take the following approach: $x = \mathrm{Fe}^{3+}/(\mathrm{Fe}^{2+} + \mathrm{Fe}^{3+})$: $\langle F \rangle_{\mathrm{Spinel}} = \frac{3x}{2}\langle F \rangle_1 + (1 - \frac{3x}{2})\langle F \rangle_2$, where $\langle F \rangle_1$ and $\langle F \rangle_2$ are estimates based on the relationship between bond length and force constant illustrated in Fig. 3b that correspond to the force constants of Ti-bonds in Ti-magnetite and ulvöspinel. For both tholeiitic and calc-alkaline magmas $\langle F \rangle_1$ and $\langle F \rangle_2$ are 296 and 309 N/m for Ti-magnetite and ulvöspinel, respectively. The force constants adopted for clinopyroxene and Rhm oxides (e.g., geikielite) are 478 and 350 N/m, respectively (Sect. 3.2)

## 4. Conclusion

The trends of titanium isotopic fractionation versus $SiO_2$ content differ significantly in calc-alkaline and tholeiitic magmatic series. These differences are attributable to variations in the nature and rate of removal of the Ti-bearing minerals that crystallize from the two magmas. In tholeiitic rocks, late onset of oxide crystallization drives the residual melt to higher $TiO_2$ concentrations while at the same time the $SiO_2$ remains nearly constant due to plagioclase crystallization. When Fe-Ti oxides start crystallizing, the $\delta^{49}$Ti value of the melt increases very rapidly even though the $SiO_2$ is relatively low. In calc-alkaline rocks, early onset of oxide crystallization and delayed onset of

plagioclase crystallization drives the $\delta^{49}$Ti value to increase more modestly while $SiO_2$ increases rapidly.

The Ti isotope composition of tholeiitic and calc-alkaline magmas undergoing fractional crystallization was modeled using the Rhyolite MELTS software, and *ab initio* derived force constants that allow us to calculate melt-mineral fractionation factors. The majority of Ti in crystallizing phases is removed via 6-fold coordinated Ti-oxides, and the Ti remaining in the melt is modeled in different coordination environments. The force constants of the crystallizing minerals and the melt proxy presented in this study along with the timing and pace of Ti-bearing mineral crystallization predicted by MELTS modeling can provide insight into the observed $\delta^{49}$Ti isotope compositions in tholeiitic versus calc-alkaline rocks. Future work should focus on constraining the differences in the coordination environment of Ti in melts with variable composition, water content, oxygen fugacity, and to a lesser degree pressure. Our results indicate that Ti isotopes, combined with other non-traditional stable isotope systematics such as Fe, can help (1) tease out the history of fractional crystallization and (2) ascribe a magma series origin, to magmas that otherwise lack geological context.

## ASSOCIATED CONTENT

**Supporting Information.** PDOS for titanium and all other elements in all minerals investigated here (xlsx), the stable titanium isotope fractionation calculated from Rhyolite MELTS model simulations and mineral-melt force constants (xlsx), and the chemical composition of ilmenite and Ti-magnetite from Kīlauea Iki lava lake mineral separates measured by SEM-EDX and the abundance of these minerals relative to total Fe-Ti oxides (xlsx).

## AUTHOR INFORMATION

### Corresponding Author

**Sarah M. Aarons**—Origins Laboratory, Department of the Geophysical Sciences and Enrico Fermi Institute, The University of Chicago, Chicago, IL, 60637, USA, and Scripps Institution of Oceanography, University of California San Diego, CA, 92093, USA

## Authors

**Nicolas Dauphas—**Origins Laboratory, Department of the Geophysical Sciences and Enrico Fermi Institute, The University of Chicago, Chicago, IL, 60637, USA
**Marc Blanchard—**Géosciences Environnement Toulouse (GET), Observatoire Midi-Pyrénées, Université de Toulouse, CNRS, IRD, CNES, UPS, 14 avenue Edouard Belin, 31400 Toulouse, France
**Hao Zeng—**Origins Laboratory, Department of the Geophysical Sciences and Enrico Fermi Institute, The University of Chicago, Chicago, IL, 60637, USA
**Nicole Xike Nie—**Earth and Planets Division, Carnegie Institution of Science, Washington DC, 20015, USA
**Aleisha C. Johnson—**Origins Laboratory, Department of the Geophysical Sciences and Enrico Fermi Institute, The University of Chicago, Chicago, IL, 60637, USA
**Nicolas D. Greber—**Institute of Geological Sciences, University of Bern, 3012, Bern, Switzerland
**Timo Hopp—**Origins Laboratory, Department of the Geophysical Sciences and Enrico Fermi Institute, The University of Chicago, Chicago, IL, 60637, USA

## Acknowledgements

This work was supported by the Ford Foundation Fellowship to SMA, NASA grants NNX17AE86G, NNX17AE87G, 80NSSC17K0744, 80NSSC20K0821, 80NSSC20K1409, and NSF grant EAR-2001098 to ND, and SNSF grant 181172 to NDG. Calculations were partly performed using the HPC resources from CALMIP (Grand 2020-P1037). Discussions with M. Roskosz, A. Heard, J. Reimink, K. Prissel, and G. Galli were greatly appreciated. All data presented in this study can be accessed in the online supplementary material.

## References

1. Barbarin, B., A review of the relationships between granitoid types, their origins and their geodynamic environments. *Lithos* **1999,** *46* (3), 605-626.
2. Moyen, J.-F.; Martin, H., Forty years of TTG research. *Lithos* **2012,** *148*, 312-336.
3. Jagoutz, O.; Kelemen, P. B., Role of Arc Processes in the Formation of Continental Crust. *Annual Review of Earth and Planetary Sciences* **2015,** *43*, 363-404.
4. Rudnick, R. L., Making continental crust. *Nature* **1995,** *378*, 571-578.
5. Grove, T. L.; Brown, S. M., Magmatic processes leading to compositional diversity in igneous rocks: Bowen (1928) revisited. *American Journal of Science* **2018,** *318*, 1-28.
6. Millet, M. A.; Dauphas, N.; Greber, N. D.; Burton, K. W.; Dale, C. W.; Debret, B.; Macpherson, C. G.; Nowell, G. M.; Williams, H. M., Titanium stable isotope investigation of magmatic processes on the Earth and Moon. *Earth and Planetary Science Letters* **2016,** *449*, 197-205.

7. Deng, Z.; Chaussidon, M.; Savage, P.; Robert, F.; Pik, R.; Moynier, F., Titanium isotopes as a tracer for the plume or island arc affinity of felsic rocks. *Proceedings of the National Academy of Sciences of the United States of America* **2019**.
8. Deng, Z.; Moynier, F.; Sossi, P. A.; Chaussidon, M., Bridging the depleted MORB mantle and the continental crust using titanium isotopes. *Geochemical Perspective Letters* **2018,** *9*, 11-15.
9. Greber, N. D.; Dauphas, N.; Bekker, A.; Ptáček, M. P.; Bindeman, I. N.; Hofmann, A., Titanium isotopic evidence for felsic crust and plate tectonics 3.5 billion years ago. *Science* **2017,** *357* (6357), 1271-1274.
10. Greber, N. D.; Dauphas, N.; Puchtel, I. S.; Hofmann, B. A.; Arndt, N. T., Titanium stable isotopic variations in chondrites, achondrites and lunar rocks. *Geochimica et Cosmochimica Acta* **2017,** *213*, 534-552.
11. Johnson, A. C.; Aarons, S. M.; Dauphas, N.; Nie, N. X.; Zeng, H.; Helz, R.; Romaniello, S. J.; Anbar, A. D., Titanium Isotopic Fractionation in Kilauea Iki Lava Lake Driven by Oxide Crystallization. *Geochimica et Cosmochimica Acta* **2019,** *264*, 180-190.
12. Hoare, L.; Klaver, M.; Saji, N. S.; Gillies, J.; Parkinson, I. J.; Lissenberg, C. J.; Millet, M. A., Melt chemistry and redox conditions control titanium isotope fractionation during magmatic differentiation. *Geochimica et Cosmochimica Acta* **2020,** *282*, 38-54.
13. Aarons, S. M.; Reimink, J. R.; Greber, N. D.; HEard, A. W.; Zhang, Z.; Dauphas, N., Titanium isotopes constrain a magmatic transition at the Hadean-Archean boundary in the Acasta Gneiss Complex. *Science Advances* **2020,** *6* (50).
14. Grove, T. L.; Baker, M. B., Phase equilibrium controls on the tholeiitic versus calc-alkaline differentiation trends. *Journal of Geophysical Research: Solid Earth* **1984,** *89* (B5), 3253-3274.
15. Miyashiro, A., Volcanic rock series in island arcs and active continental margins. *American Journal of Science* **1974,** *274*, 321-355.
16. Kuno, H., Differentiation of Basalt Magmas. In *Basalts: The Poldervaart Treatise on Rocks of Basaltic Composition*, Hess, H. H.; Poldervaart, A., Eds. Interscience Publishers: New York, 1968; pp 623-688.
17. Sisson, T.; Grove, T., Experimental investigations of the role of H2O in calc-alkaline differentiation and subduction zone magmatism. *Contributions to Mineralogy and Petrology* **1993,** *113* (143-166).
18. Kelley, K. A.; Cottrell, E., Water and the Oxidation State of Subduction Zone Magmas. *Science* **2009,** *325* (5940), 605-607.
19. Parkinson, I. J.; Arculus, R. J., The redox state of subduction zones: insights from arc-peridotites. *Chemical Geology* **1999,** *160* (409-423).
20. Teng, F.-Z.; Dauphas, N.; Helz, R. T., Iron isotope fractionation during magmatic differentiation in Kilauea Iki lava lake. *Science* **2008,** *320* (5883), 1620-1622.
21. Sossi, P. A.; Foden, J. D.; Halverson, G. P., Redox-controlled iron isotope fractionation during magmatic differentiation: an example from the Red Hill intrusion, S. Tasmania. *Contributions to Mineralogy and Petrology* **2012,** *164* (5), 757-772.
22. Weyer, S.; Seitz, H. M., Coupled lithium- and iron isotope fractionation during magmatic differentiation. *Chemical Geology* **2012,** *294-295*, 42-50.

23. Schuessler, J. A.; Schoenberg, R.; Sigmarsson, O., Iron and lithium isotope systematics of the Hekla volcano, Iceland- Evidence for Fe isotope fractionation during magma differentiation. *Chemical Geology* **2009,** *258* (1-2), 78-91.
24. Teng, F.-Z.; Dauphas, N.; Helz, R. T.; Gao, S.; Huang, S., Diffusion-driven magnesium and iron isotope fractionation in Hawaiian olivine. *Earth and Planetary Science Letters* **2011,** *308* (3-4), 317-324.
25. Farges, F.; Brown, G. E., Coordination chemistry of titanium (IV) in silicate glasses and melts: IV. XANES studies of synthetic and natural volcanic glasses and tektites at ambient temperature and pressure. *Geochimica et Cosmochimica Acta* **1997,** *61* (9), 1863-1870.
26. Farges, F.; Brown, G. E.; Rehr, J. J., Coordination chemistry of Ti (IV) in silicate glasses and melts: I. XAFS study of titanium coordination in oxide model compounds. *Geochimica et Cosmochimica Acta* **1996,** *60* (16), 3023-3028.
27. Schauble, E. A., Applying stable isotope fractionation theory to new systems. *Reviews in Mineralogy and Geochemistry* **2004,** *55* (1), 61-111.
28. Richter, F. M.; Dauphas, N.; Teng, F.-Z., Non-traditional fractionation of non-traditional isotopes: Evaporation, chemical diffusion and Soret diffusion. *Chemical Geology* **2009,** *258* (1-2), 92-103.
29. Sio, C. K. I.; Dauphas, N.; Teng, F.-Z.; Chaussidon, M.; Helz, R. T.; Roskosz, M., Discerning crystal growth from diffusion profiles in zone olivine by *in situ* Mg-Fe isotopic analyses. *Geochimica et Cosmochimica Acta* **2013,** *123*, 302-321.
30. Wang, W.; Huang, S.; Huang, F.; Zhao, X.; Wu, Z., Equilibrium inter-mineral titanium isotope fractionation: Implication for high-temperature titanium isotope geochemistry. *Geochimica et Cosmochimica Acta* **2020,** *269*, 540-553.
31. Leitzke, F. P.; Fonseca, R. O. C.; Göttlicher, J.; Steininger, R.; Jahn, S.; Prescher, C.; Lagos, M., Ti K-edge XANES study on the coordination number and oxidation state of Titanium in pyroxene, olivine, armalcolite, ilmenite, and silicate glass during mare basalt petrogenesis. *Contributions to Mineralogy and Petrology* **2018,** *173* (103).
32. Zimmer, M. M.; Plank, T.; Hauri, E. H.; Yogodzinski, G. M.; Stelling, P.; Larsen, J.; Singer, B.; Jicha, B.; Mandeville, C.; Nye, C. J., The role of water in generating the calc-alkaline trend: new volatile data for Aleutian magmas and a new tholeiitic index. *Journal of Petrology* **2010,** *51*, 2411-2444.
33. Shervais, J. W., Ti-V plots and the petrogenesis of modern and ophiolitic lavas. *Earth and Planetary Science Letters* **1982,** *59*, 101-118.
34. Grove, T. L.; Till, C. B.; Krawczynski, M. J., The role of H2O in subduction zone magmatism. *Annual Reviews Earth and Planetary Sciences* **2012,** *219* (3-4), 173-187.
35. Juster, T. C.; Grove, T. L.; Perfit, M. R., Experimental constraints on the generation of FeTi basalts, andesites, and rhyodacites at the Galapagos Spreading Center 85°W and 95°W. *Journal of Geophysical Research Solid Earth* **1989,** *94* (B7), 9251-9274.
36. Dauphas, N.; Roskosz, M.; Alp, E. E.; Golden, D. C.; Sio, C. K.; Tissot, F. L. H.; Hu, M.; Zhao, J.; Gao, L.; Morris, R. V., A general moment NRIXS approach to the determination of equilibrium Fe isotopic fractionation factors: application to goethite and jarosite. *Geochimica et Cosmochimica Acta* **2012,** *94*, 254-275.

37. Dauphas, N.; Roskosz, M.; Alp, E. E.; Neuville, D. R.; Hu, M. Y.; Sio, C. K.; Tissot, F. L. H.; Zhao, J.; Tissandier, L.; Médard, E.; Cordier, C., Magma redox and structural controls on iron isotope variations in Earth's mantle and crust. *Earth and Planetary Science Letters* **2014,** *398*, 127-140.
38. Grove, T. L.; Gerlach, D. C.; Sando, T. W., Origin of Calc-alkaline series lavas at Medicine Lake Volcano by fractionation, assimilation and mixing. *Contributions to Mineralogy and Petrology* **1982,** *80*, 160-182.
39. Müntener, O.; Ulmer, P., Arc crust formation and differentiation constrained by experimental petrology. *American Journal of Science* **2018,** *318*, 64-89.
40. Chin, E. J.; Shimizu, K.; Bybee, G. M.; Erdman, M. E., On the development of the calc-alkaline and tholeiitic magma series: A deep crustal cumulate perspective. *Earth and Planetary Science Letters* **2018,** *482*, 277-287.
41. Bland, J. A., The crystal structure of barium orthotitanate, Ba2TiO4. *Acta Crystallographica* **1961,** *14* (8), 875-881.
42. Andersson, S.; Wadsley, A. D., Crystal structure of K2Ti2O5. *Acta Chemica Scandinavica* **1961,** *15*, 663-669.
43. Abeysinghe, D.; Smith, M. D.; zur Loye, H.-C., A fresnoite-structure-related mixed valent titanium(III/IV) chlorosilicate, Ba3Ti2Si4O14Cl: A flux crystal growth route to Ti(III) containing oxides. *Journal of Solid State Chemistry* **2017,** *250*, 128-133.
44. Liferovich, R. P.; Mitchell, R. H., The pyrophanite-geikielite solid-solution series: crystal structures of the Mn1-xMgxTiO3 series (o<x<0.7). *Canadian Mineralogist* **2006,** *44*, 1099-1107.
45. Yang, H.; Hazen, R. M., Comparative high-pressure crystal chemistry of karrooite, MgTi2O5, with different ordering states. *American Mineralogist* **1999,** *84*, 130-137.
46. Pauling, L., VII. The crystal structure of pseudobrookite. *Zeitschrift für Kristallographie - Crystalline Materials* **1930,** *73* (1).
47. Taylor, M.; Brown, G. E., High-temperature structural study of the P2_1/a - A2/a phase transition in synthetic titanite, CaTiSiO5. *American Mineralogist* **1976,** *61*, 435-447.
48. Jain, A.; Ong, S. P.; Hautier, G.; Chen, W.; Richards, W. D.; Dacek, S.; Cholia, S.; Gunter, D.; Skinner, D.; Ceder, G.; Persson, K. A., Commentary: The Materials Project: A materials genome approach to accelerating materials innovation. *APL Materials* **2013,** *1* (1).
49. Rice, C. E.; Robinson, W. R., High-temperature crystal chemistry of Ti2O3: structural changes accompanying the semiconductor-metal transition. *Acta Crystallographica Section B Structural Crystallography and Crystal Chemistry* **1977,** *33* (5), 1342-1348.
50. Momma, K.; Izumi, F., VESTA 3 for three-dimensional visualization of crystal, volumetric and morphology data. *Journal of Applied Crystallography* **2011,** *44* (6), 1272-1276.
51. Giannozzi, P.; Baroni, S.; Bonini, N.; Calandra, M.; Car, R.; Cavazzoni, C.; Ceresoli, D.; Chiarotti, G. L.; Cococcioni, M.; Dabo, I.; Dal Corso, A.; de Gironcoli, S.; Fabris, S.; Fratesi, G.; Gebauer, R.; Gerstmann, U.; Gougoussis, C.; Kokalj, A.; Lazzeri, M.; Martin-Samos, L.; Marzari, N.; Mauri, F.; Mazzarello, R.; Paolini, S.; Pasquarello, A.; Paulatto, L.; Sbraccia, C.; Scandolo, S.; Sclauzero, G.; Seitsonen, A.

P.; Smogunov, A.; Umari, P.; Wentzcovitch, R. M., QUANTUM ESPRESSO: a modular and open-source software project for quantum simulations of materials. *Journal of Physics: Condensed Matter* **2009,** *21* (39), 395502.
52. Perdew, J. P.; Burke, K.; Ernzerhof, M., Generalized gradient approximation made simple. *Physical Review Letters* **1996,** *77* (18), 3865.
53. Schlipf, M.; Gygi, F., Optimization algorithm for the generation of ONCV pseudopotentials. *Computer Physics Communications* **2015,** *196* (36-44).
54. Monkhorst, H. J.; Pack, J. D., Special points for Brillouin-zone integrations. *Physical Review B* **1976,** *13* (12), 5188-5192.
55. Ghiorso, M. S.; Gualda, G. A., An H2O-CO2 mixed fluid saturation model compatible with rhyolite-MELTS. *Contributions to Mineralogy and Petrology* **2015,** *169* (6), 53.
56. Gualda, G. A. R.; Ghiorso, M. S.; Lemons, R. V.; Carley, T. L., Rhyolite-MELTS: A modified calibration of MELTS optimized for silica-rich, fluid-bearing magmatic systems. *Journal of Petrology* **2012,** *53*, 875-890.
57. Young, E. D.; Manning, C. E.; Schauble, E. A.; Shahar, A.; Macris, C. A.; Lazar, C.; Jordan, M., High-temperature equilibrium isotope fractionation of non-traditional stable isotopes: Experiments, theory, and applications. *Chemical Geology* **2015,** *395*, 176-195.
58. Nie, N. X.; Dauphas, N.; Alp, E. E.; Zeng, H.; Sio, C. K.; Hu, J. Y.; Chen, X.; Aarons, S. M.; Zhang, Z.; TIan, H.-C.; Wang, D.; Prissel, K. B.; Greer, J.; Bi, W.; Hu, M. Y.; Zhao, J.; Shahar, A.; Roskosz, M.; Teng, F.-Z.; Krawczynski, M. J.; Heck, P. R.; Spear, F. S., Iron, magnesium, and titanium isotopic fractionations between garnet, ilmenite, fayalite, biotite, and tourmaline: Results from NRIXS, *ab initio*, and study of mineral separates from the Moosilauke metapelite. *Geochimica et Cosmochimica Acta* **2021,** *302*, 18-45.
59. Greber, N. D.; Pettke, T.; Vilela, N.; Lanari, P.; Dauphas, N., Titanium isotopic composition of bulk rock and mineral separates from the Kos magmatic suite: insights into fractional crystallization and magma mixing processes. *Chemical Geology* **2021,** *578* (120303).
60. Shen, C.; Zhang, H.; Cong, H.; Yu, H.; Wang, J.; Zhang, S., Investigations on the thermal and piezoelectric properties of fresnoite Ba2TiSi2O8 single crystals. *Journal of Applied Physics* **2014,** *116* (044106).
61. Nazzareni, S.; Molin, G.; Skogby, H.; Dal Negro, A., Crystal chemistry of Ti3+-Ti4+-bearing synthetic diopsides. *European Journal of Mineralogy* **2004,** *16* (3), 443-449.
62. Smyth, J. R.; Jacobsen, S. D.; Hazen, R. M., Comparative Crystal Chemistry of Dense Oxide Minerals. *Reviews in Mineralogy and Geochemistry* **2000,** *41* (1), 157-186.
63. Speer, J. A.; Gibbs, G. V., The crystal structure of synthetic titanite, CaTiOSiO4, and the domain textures of natural titanites. *American Mineralogist* **1976,** *61* (3-4), 238-247.
64. de Groot, F. M. F.; Figueiredo, M. O.; Basto, M. J.; Abbate, M.; Petersen, H.; Fuggle, J. C., 2p X-ray Absorption of Titanium in Minerals. *Physical Chemistry Minerals* **1992,** *19*, 140-147.
65. Bosi, F.; Halenius, U.; Skogby, H., Crystal chemistry of the magnetite-ulvöspinel series. *American Mineralogist* **2009,** *94*, 181-189.

66. Merazka, S.; Hammoudi, L.; Kars, M.; Sidoumou, M.; Roisnel, T., Structure and New Substructure of α-Ti2O3: X-ray Diffraction and Theoretical Study. *Journal of Modern Materials* **2021,** *8* (1), 3-11.
67. Burdett, J. K.; Hughbanks, T.; Miller, G. J.; Richardson Jr., J. W.; Smith, J. V., Structural-electronic relationships in inorganic solids: powder neutron diffraction studies of the rutile and anatase polymorphs of titanium dioxide at 15 and 295 K. *Journal of the American Chemical Society* **1987,** *109* (12), 3639-3646.
68. Mandl, M. B. Titanium isotope fractionation on the Earth and Moon: Constraints on magmatic processes and Moon formation. ETH Zurich, 2019.
69. Rzehak, L. J. A.; Kommescher, S.; Kurzweil, F.; Sprung, P.; Leitzke, F. P., The redox dependence of titanium isotope fractionation in synthetic Ti-rich lunar melts. *Contributions to Mineralogy and Petrology* **2021,** *176* (19).
70. Keller, C. B.; Schoene, B., Statistical geochemistry reveals disruption in secular lithospheric evolution about 2.5 Gyr ago. *Nature* **2012,** *485* (7399), 490-493.
71. Quartieri, S.; Antonioli, G.; Artioli, G.; Lottici, P. P., XANES study of titanium coordination in natural diopsidic pyroxenes. *European Journal of Mineralogy* **1993,** *5* (6), 1101-1109.
72. Fujino, K., Cation distribution and local variation of site symmetry in solid solution series, Fe3O4-Fe2TiO4. *Mineralogical Journal* **1974,** *7*, 472-488.
73. Wechsler, B. A.; Lindsley, D. H.; Prewitt, C. T., Crystal structure and cation distribution in titanomagnetites (Fe3-xTixO4). *American Mineralogist* **1984,** *69*, 754-770.
74. Pearce, C. I.; Henderson, C. M. B.; Telling, N. D.; Pattrick, R. A. D.; Charnock, J. M.; Coker, V. S.; Arenholz, E.; Tuna, F.; van der Laan, G., Fe site occupancy in magnetite-ulvöspinel solid solutions: A new approach using X-ray magnetic circular dichroism. *American Mineralogist* **1995,** *95* (4), 425-439.
75. Pearce, C. I.; Henderson, C. M. B.; Pattick, R. A. D.; van der Laan, G.; Vaughan, D. J., Direct determination of cation site occupancies in natural ferrite spinels by L2,3 x-ray absorption spectroscopy and x-ray magnetic circular dichroism. *American Mineralogist* **2006,** *92*, 880-893.
76. Gatta, G. D.; Bosi, F.; McIntyre, G. J.; Hålenius, U., Static positional disorder in ulvöspinel: A single-crystal neutron diffraction study. *American Mineralogist* **2014,** *99*, 255-260.
77. Liu, H.; Di Valentin, C., Band gap in magnetite above Verwey temperature induced by symmetry breaking. *Journal of Physical Chemistry C* **2017,** *121*, 25736-25742.
78. Chen, X.; Wang, W.; Zhang, Z.; Nie, N. X.; Dauphas, N., Evidence from *Ab Initio* and Transport Modeling for Diffusion-Driven Zirconium Isotopic Fractionation in Igneous Rocks. *ACS Earth and Space Chemistry* **2020,** *4*, 1572-1595.

for TOC only

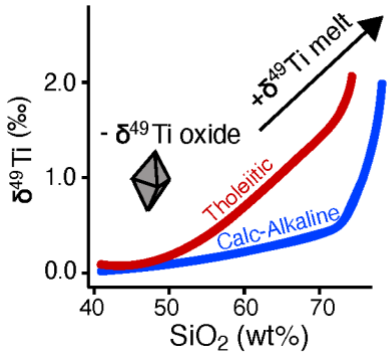
+δ49Ti melt
- δ49Ti oxide
Tholeiitic
Calc-Alkaline
δ49Ti (‰)
2.0
1.0
0.0
40
50
60
70
SiO2 (wt%)